REPORT DOCUMENTATION PAGE

Form Approved
OMB NO. 0704-0188

1. AGENCY USE ONLY (Leave Blank)	2. REPORT DATE 9/14/03	3. REPORT TYPE AND DATES COVERED Final report. 9/15/00-~~9/14/03~~ 6/14/03
4. TITLE AND SUBTITLE Development of a Discharge Pumped 13nm laser for metrology of projection lithography optics at the manufacture-site		5. FUNDING NUMBERS ~~G~~-DAAD 19-99-1-0279
6. AUTHOR(S) Jorge J. Rocca		
7. PERFORMING ORGANIZATION NAME(S) AND ADDRESS(ES) Colorado State University Fort Collins, CO 80523		8. PERFORMING ORGANIZATION REPORT NUMBER Four
9. SPONSORING / MONITORING AGENCY NAME(S) AND ADDRESS(ES) U. S. Army Research Office P.O. Box 12211 Research Triangle Park, NC 27709-2211		10. SPONSORING / MONITORING AGENCY REPORT NUMBER ~~ARO~~ 40300.1-EL

11. SUPPLEMENTARY NOTES

The views, opinions and/or findings contained in this report are those of the author(s) and should not be construed as an official Department of the Army position, policy or decision, unless so designated by other documentation.

12 a. DISTRIBUTION / AVAILABILITY STATEMENT	12 b. DISTRIBUTION CODE
Approved for public release; distribution unlimited.	

13. ABSTRACT (Maximum 200 words)

A high power capillary discharge cadmium plasma source was developed to investigate the generation of 13.2 nm coherent radiation for metrology tasks in Extreme Ultraviolet Lithography. Excitation of a capillary channel filled with Cd vapor with a fast current pulse (190 kA, 15 ns risetime) resulted in the successful excitation of 13.2 nm radiation from the 4d 1S0 – 4p 1P1 laser line of Nickel-like Cd (Cd XXI). Spectra of this capillary discharge plasma showed the emission from the 13.2nm laser line is the most intense in that spectral region. Detailed spectroscopic studies confirmed that the observed 13.2 nm line radiation corresponds to the Cd XXI laser line, and identified fifty-five Cd XXI lines in the 12.7-18.4 nm region which constitute a valuable diagnostics to optimize the gain in the 13.2 nm laser line using line intensity ratio techniques. The dynamics and symmetry of the capillary discharge Cd plasma column were also studied using an EUV pinhole camera . The pinhole images show that the plasma column presents a good degree of symmetry up to the time of maximum compression.

14. SUBJECT TERMS Extreme Ultraviolet Radiation. Capillary discharge lasers			15. NUMBER OF PAGES 35
			16. PRICE CODE
17. SECURITY CLASSIFICATION OR REPORT **UNCLASSIFIED**	18. SECURITY CLASSIFICATION ON THIS PAGE **UNCLASSIFIED**	19. SECURITY CLASSIFICATION OF ABSTRACT **UNCLASSIFIED**	20. LIMITATION OF ABSTRACT **UL**

NSN 7540-01-280-5500 **Standard Form 298 (Rev.2-89)**
Prescribed by ANSI Std. 239-18 298-102

GENERAL INSTRUCTIONS FOR COMPLETING SF 298

The Report Documentation Page (RDP) is used for announcing and cataloging reports. It is important that this information be consistent with the rest of the report, particularly the cover and title page. Instructions for filling in each block of the form follow. It is important to ***stay within the lines*** to meet ***optical scanning requirements.***

This information is in the attached file "AnnualreportG-DAAD199910279.pdf"

Enclosure 2

MASTER COPY: PLEASE KEEP THIS "MEMORANDUM OF TRANSMITTAL" BLANK FOR REPRODUCTION PURPOSES. WHEN REPORTS ARE GENERATED UNDER THE ARO SPONSORSHIP, FORWARD A COMPLETED COPY OF THIS FORM WITH EACH REPORT SHIPMENT TO THE ARO. THIS WILL ASSURE PROPER IDENTIFICATION. NOT TO BE USED FOR INTERIM PROGRESS REPORTS; SEE PAGE 2 FOR INTERIM PROGRESS REPORT INSTRUCTIONS.

Table of Contents

Final Report

Grant: G-DAAD 19-99-1-0279

"Development of a Discharge Pumped 13nm laser for metrology of projection lithography optics at the manufacture-site"

PI: Jorge J. Rocca
Colorado State University

I. Summary

Statement of Problem studies and results

A high power capillary discharge cadmium plasma source was developed for the generation of 13.2 nm coherent radiation for metrology in Extreme Ultraviolet Lithography. Excitation of a capillary channel filled with Cd vapor with a fast current pulse resulted in the successful excitation of 13.2 nm radiation from the 4d $^1S_0$ – 4p $^1P_1$ laser line of Nickel-like Cd. Spectra of this capillary discharge plasma showed the emission from the 13.2nm laser line is the most intense in that spectral region. This approach for the generation of extreme ultraviolet radiation consists in the excitation of Nickel -like Cd ions (Cd XXI) by collisional electron impact excitation in a dense capillary discharge plasma channels heated by a fast discharge current pulse. The experiments were conducted using a novel high power capillary discharge set-up specifically developed to explore amplification at the wavelengths of interest for EUV lithography. Cd vapor generated by a pulsed metal-vapor source is injected into a capillary discharge channel where it is excited with current pulses of < 15 ns risetime and peak amplitude of up to 190 kA. The current pulses were generated by a scheme consisting of three-pulse compression stages, the last of which is a multi-switch Blumlein transmission line. Detailed spectroscopic studies were conducted to confirm that the observed 13.2 nm line radiation corresponds to the Cd XXI laser line. Fifty-five Cd XXI lines were identified for the first time in the 12.7-18.4 nm region with the assistance of calculations performed using the Slater-Condon method with generalized least-squares fits of the energy parameters. Many of these transitions had not been previously observed, and have been assigned for the first time as the result of this work. These spectroscopy results a valuable tool to optimize the gain in the 13.2 nm laser line using line intensity ratio techniques. The dynamics and symmetry of the capillary discharge Cd plasma column was also studied using an EUV pinhole camera with a temporal resolution better than 3 ns. The pinhole images show that the plasma column presents a good degree of symmetry up to the time of maximum compression. The results were compared with hydrodynamic model simulations.

In addition to the experiments for the generation 13.2 nm emission from Ni-like Cd, spectroscopy studies were also conducted to investigate the generation of 13.9 nm radiation by excitation of the 4d $^1S_0$ – 4p $^1P_1$ laser line of Nickel-like Ag, which model calculations suggest should have a larger gain than the equivalent transition in Ni-like Cd. The study of the Ni-like silver (Ag XX) spectra in the 13.7 -20.5 nm wavelength region identified emission from the 13.9nm laser line and other forty-two Ag XX transitions, demonstrating that high power capillary

discharge plasmas are capable of exciting Ni-like ions for the generation of radiation in the 13.5 nm spectral region.

II. Summary of the most important project results

The main results of the project include:

1) The generation of emission from the 13.2 nm radiation from the laser line of Ni-like Cd by electron impact excitation of Cd vapor in a high power capillary discharge plasma. This result is discussed in the attached reference 1 and 6. Figure.4 in the attached paper by A. Rahman et al. (ref.1) shows an axial spectrum of the Cd plasma column in which the $4d\ ^1S_0 - 4p\ ^1P_1$ laser line of Cd XXI. is dominant.

2). The successful development of a high power capillary discharge, capable of delivering current pulses of < 15 ns risetime and 200 KA peak amplitude through a capillary load for the excitation of laser transitions in the vicinity of 13.5 nm. A description of this discharge generator is given in the attached paper by J. Gonzalez et al. published in Physical Review E.(Ref. 2).

2) The generation of highly ionized dense plasma columns in Ar gas . The results of spectroscopic studies, extreme ultraviolet pinhole camera images and modeling confirmed that this type of discharge can reach plasma temperatures (> 250 eV) and densities (> 1 10^{20} cm^{-3}) that are required for the development of a 13nm discharge pumped laser. Experimental and model results of the generation of highly ionized plasma columns in Ar are summarized in the attached Phys. Rev. E paper by J. Gonzalez et al. (Ref2).

3) The generation of highly ionized plasma columns in Cd vapor. Spectroscopy of Cd plasma columns generated in a capillary channel filled with Cd vapor generated by a pulsed metal vapor source identified emission from numerous Ni-like Cd lines. Fifty-five CdXXI lines were identified for the first time in the 12.7-18.4 nm region with the assistance of calculations performed using the Slater-Condon method with generalized least-squares fits of the energy parameters. Many of these transitions had not been previously observed, and have been assigned for the first time as the result of this work. The results are discussed in the attached paper by A. Rahman et al. in Physica Scripta , 2003 (Ref.3).

4) The study of the evolution of the highly ionized plasma columns using an extreme ultraviolet pinhole camera. The results show that the plasma column displays a good degree of symmetry up to the time of maximum plasma compression. The results are discussed in the attached paper . “Excitation of the 13.2 nm laser line of Nickel-like Cd in a capillary discharge plasma column” by A. Rahman et al. (Ref. 1 and Ref. 6).

6) Spectroscopy of a highly ionized Ag plasma column. The study is motivated by the possibility of obtaining amplification in the 13.9 nm line of Nickel-like Ag. This Ag transition, which is also in the spectral range that can be useful for metrology for EUV lithography, provides an alternative source of laser radiation to the Ni-like Cd transition. Model computations suggest the gains should be larger in the Nickel-like Ag line provided the optimum plasma conditions for gain can be achieved in a Ag capillary discharge plasma column (see fig.4. in ref 5). However,

the Ag scheme has the additional difficulty that Ag is more difficult to vaporize. The work has resulted in the identification of emission from more than 30 transitions from Nickel like Ag, including the observation of the laser line at 13.9 nm (Ref. 8).

7). A new technique to measure the density and distribution of a metal vapor column was developed. Knowledge of the density and uniformity of the Cd vapor within the capillary is crucial for achievement of large amplification of the laser line. For this purpose we utilized the beam from a 46.9nm capillary discharge laser to measure the Cd metal vapor density in the column by the method of photoionization absorption. Results indicate that for large amplification of the 13.2 nm laser line the density of metal vapor need to be increased.

A list of selected publications discussing these results are attached

III. Publications reporting results of the work done under Grant: G-DAAD 19-99-1-0279

1. A. Rahman, E.C. Hammarsten, S. Sakadzic, J.J. Rocca, V.N. Shlyaptsev, A. Osterheld and J.-F. Wyart. "Excitation of the 13.2 nm laser line of Nickel-like Cd in a capillary discharge plasma column". p 113, "X-Ray Lasers 2002". Proc. 8th International Conference on X-Ray Lasers,. Editors J.J. Rocca, J. Dunn and S. Suckewer, AIP Conf. Proc. **641** (2002)

2. J.J. Gonzales, M. Frati, J.J. Rocca, V.N. Shlyaptsev and A. Osterheld. "High power density capillary discharge plasma column for shorter wavelength discharge-pumped soft x-ray lasers". Physical Review E. **65**, 026404, (2002).

3. A. Rahman, E.C. Hammarsten, S. Sakadzic, J.J. Rocca, and J.-F. Wyart "Identification of n = 4, ? n = 0 transitions in the spectra of Nickel-like Cadmium ions from a capillary discharge plasma column". Physica Scripta, **67**, 414, (2003).

4. J.J. Rocca, B. Luther, M.C. Marconi, T. Whiteaker, D. A. Braley, J. Filevich, E.C. Hammearsten. A. Rahman, B.T. Szapiro, Y. Wang, E. Jankowska and M. Grisham. "Extremely compact capillary dischage-based soft x-ray laser development and application to dense plasma diagnostics" p 125, Proc. 8th International Conference on X-Ray Lasers. Editors J.J. Rocca, J. Dunn and S. Suckewer , AIP Conf. Proc. **641** (2002.

5. V.N. Shlyaptsev, et al. "Exploring the potential of table-top x-ray lasers and capillary discharges for applications". p 528 in X-Ray Lasers 2002. Proc. 8th International Conference on X-Ray Lasers, AIP Conf. Proc. **641** (2002).

6. S. Sakadzic, A. Rahman, M. Frati, F.G. Tomasel, J.J. Rocca, V.N. Shlayptsev and A. Osterheld. "Observation of the 13.2nm laser line of nickel-like Cd in a capillary discharge". SPIE vol. 4505. Editors E. Fill and J.J. Rocca. (2001).

7. M. Frati, F.G. Tomasel, B. Bowers, J.J. Gonzalez, V.N. Shlyaptsev and J.J. Rocca. "Generation of highly ionized cadmium plasma columns for a discharge-pumped Nickel-like Cd laser". Journal de Physique IV ,571, **11**, (2001)

8. A. Rahman, J.J. Rocca, and J-F Wyart, “Classification of the Nickel-like Silver Spectrum from a Fast Capillary Discharge Plasma”, Submitted to Physica Scripta, Sept. (2003)

IV. List of participating scientific personnel

- Prof. Jorge J. Rocca
- Dr. Fernando Tomasel
- Mr. Maximo Frati (Completed Master of Science Degree in Electrical and Computer Engineering)
- Mr. Eric Hammarsten (Completed Master of Science Degree in Electrical and Computer Engineering, fall 2003)
- Mr. Sava Sakadzic
- Abdur Rahman
- Vyacheslav Shlyaptsev

Excitation of the 13.2 nm laser line of Nickel-like Cd in a capillary discharge plasma column

A. Rahman, E.C. Hammarsten, S. Sakadzic, J.J. Rocca
Colorado State University. Fort Collins, CO 80523,
V.N. Shlyaptsev [a,b] and A. Osterheld[a]
Lawrence Livermore National Laboratory [a]/University of California Davis [b]
J.-F. Wyart
Laboratoire Aime Cotton, CNRS (UPR 3321)
Centre Universitaire 91405 - Orsay (France)

Abstract. Emission at 13.2 nm from the 4d $^1S_0$ -4p $^1P_1$ laser transition of Ni-like Cd was observed in a cadmium vapor plasma column excited by a high-current capillary discharge. The dynamics of the plasma were studied using time-resolved soft x-ray pinhole images and hydrodynamic simulations. The pinhole images show that the plasma column maintains a good symmetry up to the time of maximum compression. Fifty-five CdXXI lines were identified in the 12.7-18.4 nm region with the assistance of calculations performed using the Slater-Condon method with generalized least-squares fits of the energy parameters.

INTRODUCTION

Capillary discharge excitation has been demonstrated to be a very successful method for the generation of compact and efficient soft x-ray lasers [1-5]. Large amplification in capillary discharge-pumped ultra short wavelength lasers has been achieved in Ne-like Ar, Ne-like S and Ne-like Cl at wavelengths ranging from 46.9 nm to 60.8 nm [1-3]. Utilizing this excitation technique a high repetition rate tabletop laser operating at 46.9 nm has produced the highest average power reported to date for a soft x-ray laser, 3.5 mW [4], and it has been successfully utilized in several applications [5]. There is significant interest in the possibility of extending capillary discharge lasers to shorter wavelengths. Of particular interest is the possibility of obtaining lasing near 13.5 nm, a wavelength that is of interest for extreme ultraviolet lithography [6]. Scaling of the collisional laser scheme to this wavelength can be accomplished by the excitation of Nickel-like Cd ions (CdXXI), which can provide amplification at 13.2nm in the 4d $^1S_0$ -4p $^1P_1$ transition [7]. However, excitation of the laser upper level of Ni-like Cd requires a large increase in the discharge excitation power with respect to that used to produce lasing in the 46-61 nm region. We have developed a high power capillary discharge capable of generating the hotter and denser plasmas that are necessary for this task [8]. This pulsed power generator produces pulses of up to 200 kA with a 10-90% rise time of less than 15 ns. The initial study of the generation of hot dense plasmas with this high power capillary discharge involved the excitation of Ar gas, which resulted in electron temperatures of > 250 eV and electron densities of ~ 1×10^{20} cm^{-3} [8].

In this proceedings we discuss results of the generation of highly ionized cadmium plasma columns for amplification in Ni-like Cd, including the observation of strong line emission from the 13.2 nm laser transition. The dynamics of the column was studied using

time-resolved soft x-ray pinhole images and model simulations. Spectroscopy of the plasma column in the 12.7-18.4 nm region resulted in the classification of fifty-five $3d^9$ 4p-$3d^9$ 4d and $3d^9$ 4d- $3d^9$ 4f Cd XXI lines.

GENERATION OF HIGHLY IONIZED CD PLASMA COLUMNS

The plasma columns were generated by exciting a capillary channel filled with Cd vapor with a fast high current pulse. Cd vapor was generated by a metal vapor gun, designed to generate vapor in a room temperature environment by rapidly heating a cadmium electrode with a capacitive discharge, and was injected into the capillary channel though an axial hole in one of the electrodes. The high current pulses used to excite the capillary plasma were produced by a pulse power generator consisting of a three-stage pulse compression scheme. The first stage, which produces a current pulse that is subsequently shorten by each of two following stages, consists of a conventional eight stage Marx generator that for the present experiment was operated at an erected voltage of ~ 650 kV. The Marx generator is used to charge the second pulse compression stage that consists of a 26 nF coaxial water-dielectric capacitor in about 1 μs. In turn this water capacitor is discharged through a self-breakdown spark gap pressurized with SF_6 gas to charge the third and final stage in about 75 ns. The third stage consists of two radial water dielectric transmission lines connected in a Blumlein configuration. The capillary channel is located at the axis of this radial Blumlein. The fast current pulse that excites the capillary plasma is produced by discharging the Blumlein transmission line through an array of seven synchronized triggered spark-gap switches distributed along the outer diameter of the water transmission line. The very rapid switching of the Blumlein transmission line produces current pulses with amplitudes of up to 200 kA and risetimes of less than 15 ns through the capillary load.

DYNAMICS OF THE CADMIUN PLASMA COLUMN

The evolution and stability of the Cd plasma columns was studied using a soft x-ray pinhole camera equipped with a microchannel plate MCP-CCD detector. The set up provided a magnification of 2.76 times. Gating of the MCP allowed for images of the plasma column with ~ 3 ns temporal resolution. A combination of a 1 μm thick carbon filter and a 0.2 μm thick aluminum filter was used to limit the response of the camera to photons with wavelengths between 45 Å and 100 Å and below 20 Å, allowing for the differentiation of the hotter regions of the plasma from the colder regions that emit longer wavelength radiation. Figure 1 consists of a sequence of end-on images of the plasma column, showing the evolution of the soft x-ray-emitting region of the Cd plasma in a 2.5 cm long polyacethal capillary of diameter 5 mm. The time of each image with respect to the initiation of the current pulse is indicated. The images show that the onset of significant soft x-ray emission occurs about 27 ns after the initiation of the current pulse, with rapidly increasing intensity in the few nanoseconds after that. The diameter of the soft x-ray emitting regions achieves a minimum diameter of 250-350 μm at 32-34 ns after the onset of the current pulse. Shortly afterwards the emitted soft x-ray intensity rapidly decreases. The plasma column is observed to have a good degree of symmetry, comparable to that observed in the plasma columns of the Ne-like Ar laser. This occurs up to the time of maximum compression. Later in time the plasma becomes asymmetrical. However, these

late un-uniformities should not be of concern for soft x-ray laser development because they appear after the time of interest for laser amplification.

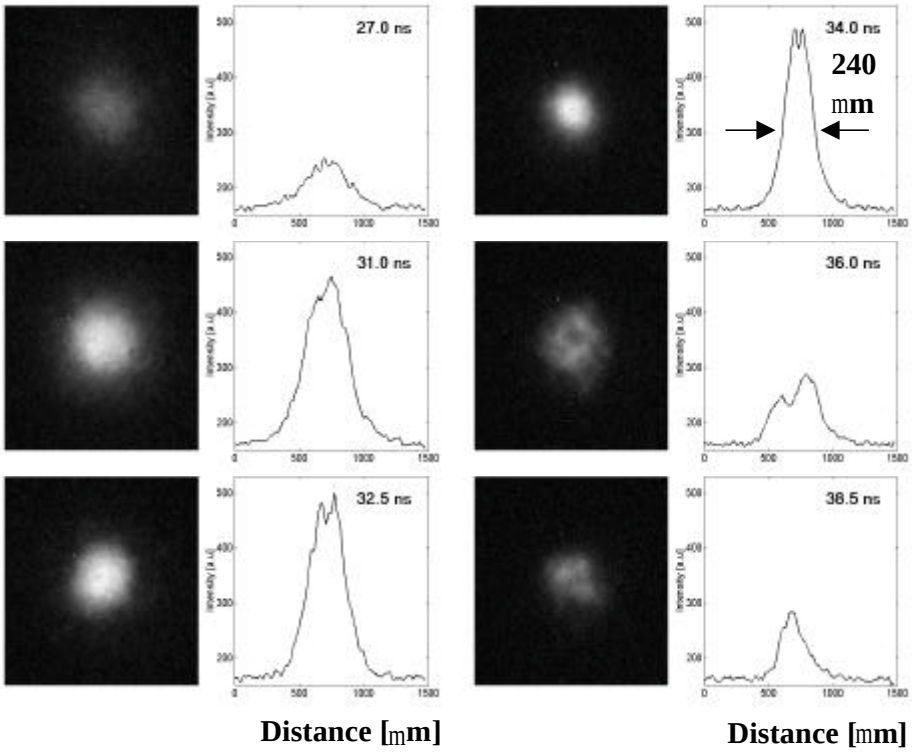

Figure 1. Sequence of end-on pinhole images of the soft x-ray emitting region of the Cd plasma column acquired using a 1 μm thick carbon filter and a 0.2 μm thick aluminum filter. The time of each image with respect to the initiation of the current pulse is indicated. The discharge current was ~190 kA and the capillary diameter was 5 mm.

These experimental observations are in good agreement with hydrodynamic model simulations conducted using RADEX. Results corresponding to a 190 kA cadmium discharge in a 4 mm diameter capillary at a Cd pressure of 0.9 Torr are shown in figure 2. The graphs of the evolution of the computed plasma parameters shows the dynamics of a cylindrical shock wave shell that is driven towards the axis of the discharge by the Lorentz force and thermal pressure in the skin layer near the walls. The electron temperature plot shows that the heat wave moves ahead of the mass, pre-heating the plasma in front of the shock wave. When this heat wave reaches the axis, the maximum of the current density switches to the center of the capillary, and the temperature rapidly increases. The main amount of the mass in the plasma shell is computed to reach the axis of the capillary several nanoseconds later (see electron density graph, Fig 2.). The electron density is calculated to reach a maximum value of 1–2 $\times 10^{20}$ cm^{-3}. It is also interesting to notice that due to maximum joule heating on axis the computed electron density profile has a concave radial profile that could potentially guide the laser beam. Preliminary computations estimate the gain in the 13.2 nm line of Ni-like Cd at 1-2 cm^{-1}, and potentially > 3 cm^{-1} under optimized excitation conditions. The simulation results are further discussed in another paper in these proceedings [9].

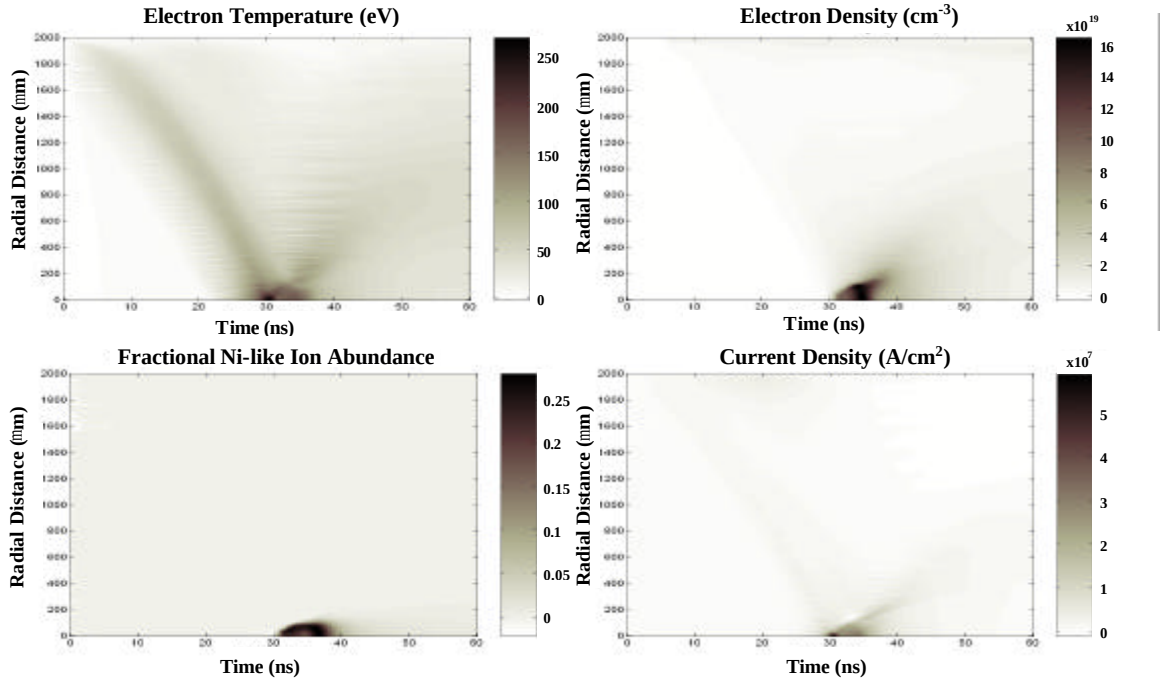

Figure 2. Computed evolution of the plasma parameters of the Cd capillary discharge plasma column. The graphs show the evolution of the electron temperature, electron density, density of Ni-like ions, and the current density. The peak discharge current is 190 kA, the capillary diameter is 4 mm and the initial cadmium pressure is 0.9 Torr.

SPECTROSCOPY: OBSERVATION OF EMISSION FROM THE 4d $^1S_0$- 4p $^1P_1$ LASER LINE OF Ni- LIKE Cd AND NEWLY IDENTIFIED CdXXI LINES

Time resolved spectroscopy of the Cd plasma column was carried out through selected intervals in the spectral range between 12.7 nm and 18.4 nm. The radiation axially emitted by the plasma was focused by a gold-coated grazing-incidence mirror into the slit of a 2.217 m grazing-incidence spectrograph with a 2400 lines per millimeter gold-coated diffraction grating. Figure 3 shows end-on spectra of the capillary discharge plasma for 15.5-16.6 and 17.2-18.4 nm regions. The spectra are observed to be dominated by lines from Ni-like (CdXXI) and Cu-like (CdXX) ions. From these and other spectra we identified fifty five lines corresponding to $3d^9$ 4p-$3d^9$ 4d and $3d^9$ 4d- $3d^9$ 4f CdXXI transitions with the assistance of calculations performed using the Slater-Condon method with generalized least-squares fits (GLS) of the energy parameters [10]. The average deviation between the measured and theoretical wavelengths is $\langle\lambda exp-\lambda th\rangle$ = 0.0065 nm. The dassification of lines of Nickel-like CdXXI is shown in Figure 3. The measured transition wavelength (in Å) is followed by the level designation given as the J-value and index N_{th}, which numbers the levels from the lowest energy in the same J-values and configuration, as used in [10]. Figure 4 shows strong line emission observed at (13.162 ± 0.010) nm which is assigned to correspond to the 4d $^1S_0$ -4p $^1P_1$ laser line of Ni-like Cd (this value is more accurate than our previously reported wavelength of 13.172 nm). This measured wavelength agrees well with the previously reported wavelength (13.166 ± 0.015) nm of this line [7]. It also is in good agreement with the computed GLS theoretical value of 13.1719 nm.

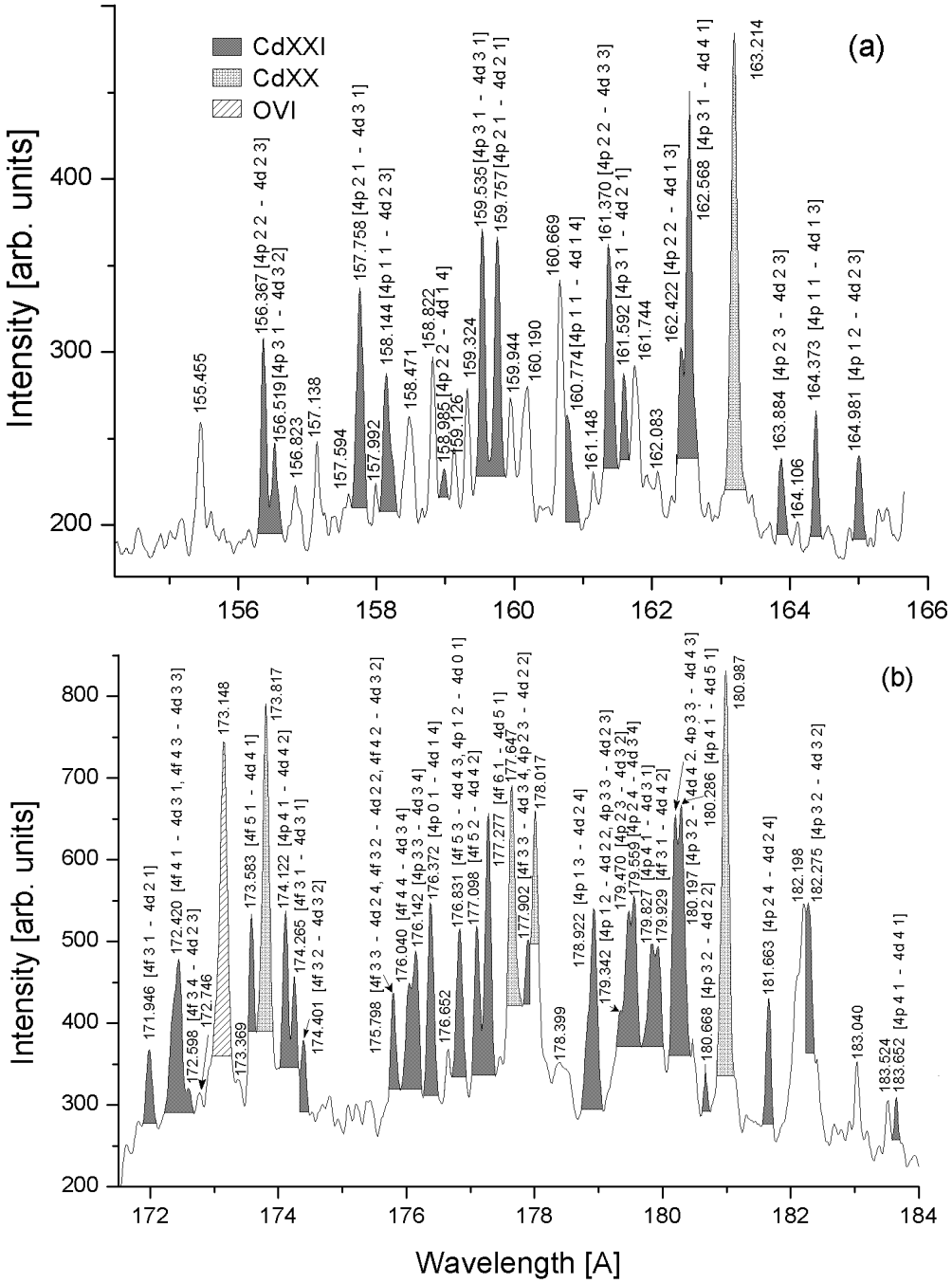

Figure 3. On axis spectra of a cadmium capillary discharge plasma column obtained at discharge currents of ~ 180 kA, and a capillary diameter of 5 mm. The measured transition wavelength (in Å), is followed by the level designation given as the J-value and the index level N_{th}. For some lines the wavelength values is the average of two spectra.

CONCLUSIONS

In summary, we have demonstrated that a fast capillary discharge is capable of generating radially symmetric plasma columns of small diameter in which Cd atoms are ionized to the

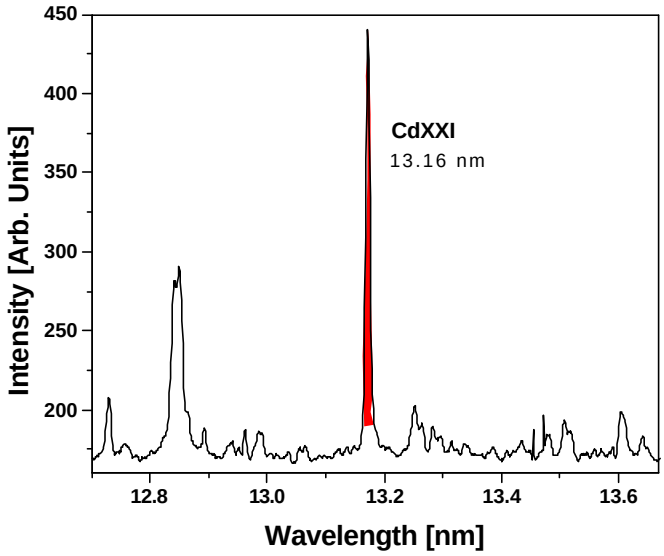

Figure 4. On axis spectra of the Cd capillary discharge plasma showing emission from the 13.2 nm line of Ni-like Cd.

Ni-like stage. Axial spectra of the discharge identified strong line emission at 13.2 nm, corresponding to the 4d $^1S_0$- 4p $^1P_1$ laser transition of Ni-like Cd. This identification is supported by the simultaneous observation of numerous Ni-like Cd lines. These results advance the possibility of the demonstration of a discharge-pumped laser in this transition, and in laser lines of other Nickel-like ions.

ACKNOWLEDGMENTS

This work was supported by DARPA grant DAAD 19-99-1-0279 and by the National Science Foundation. We also gratefully acknowledge the support of the W.M. Keck Foundation and the earlier contributions of F. Tomasel and M. Frati.

REFERENCES

1. J.J. Rocca**,** V. N. Shlyaptsev, F.G. Tomasel, O.D. Cortazar, D. Hartshorn, J.L.A. Chilla,, Phys. Rev. Lett., **73**, 2192, 1994; J.J. Rocca, D.P.Clark, J.L.A. Chilla, and V.N. Shlyaptsev, Phys. Rev. Lett. **77**, 1476-1479, (1996).
2. F.G. Tomasel, J.J.Rocca, V.N. Shlyaptsev, and C.D. Macchietto, Phys. Rev. A **55,** 1437-1440 (1997).
3. M. Frati, M. Seminario, and J.J. Rocca, Opt. Lett. **25**, 1022-1024 (2000).
4. C. Macchietto, B.R. Benware and J.J. Rocca, Opt. Lett. **24**, 1115-1117, (1999).
5. J.J. Rocca, et. al., Comptes Rendus De L' Academie Des Sciences Serie IV, Physique Astrophysique, **8**, 1065-1081 (2000).
6. D.T. Attwood, X-Ray Lasers, 2000 – J. Phys. IV **1**, Pr2-443-449 (2001).
7. Y. Li, J. Nilsen, J. Dunn, and A. L. Osterheld, Physical Review **A 58**, R2668 – 2672 (1998).
8. J.J. Gonzalez, M. Frati, Rocca J.J. and V.N. Shlyaptsev, and A.L. Osterheld, Phys. Rev E. **65**, 026404, (2002).
9. V.N. Shlyaptsev, et al., in these Proceedings
10. S.S. Churilov, A.N. Ryabtsev, and J.-F. Wyart, Physica Scripta **38**,326-35 (1988).

High-power-density capillary discharge plasma columns for shorter wavelength discharge-pumped soft-x-ray lasers

J. J. Gonzalez, M. Frati, and J. J. Rocca*
Department of Electrical and Computer Engineering, Colorado State University, Fort Collins, Colorado 80523

V. N. Shlyaptsev
Department of Applied Sciences, UC Davis-Livermore, Livermore, California 94550
and Lawrence Livermore National Laboratory, Livermore, California 94550

A. L. Osterheld
Lawrence Livermore National Laboratory, Livermore, California 94550
(Received 4 June 2001; published 24 January 2002)

We report the generation of plasma columns in gas-filled capillary channels using discharge excitation powers that exceed those of previous studies by one to two orders of magnitude. Current pulses up to 200 kA and 10–90 % rise time of ~10 ns (current increase rate $\sim 1.5\times 10^{13}$ A/s) were utilized to excite plasmas in 3.3 and 4 mm diameter channels. Time resolved soft-x-ray spectra and pinhole images of the plasma were obtained. The experimental data and its comparison with model computations suggest that dense argon plasma columns 300 μm in diameter with electron temperatures >250 eV have been obtained. These characteristics make these plasmas of interest for extending discharge-pumped lasers to shorter wavelengths.

DOI: 10.1103/PhysRevE.65.026404 PACS number(s): 52.80.−s, 42.55.−f

I. INTRODUCTION

There is significant interest in the development of practical soft-x-ray lasers for applications [1]. Excitation approaches include the use of high power lasers and fast capillary discharges [1–10]. Fast capillary discharges have been demonstrated to efficiently generate highly uniform plasma columns of small diameter [11,13], in which large soft-x-ray amplification has been obtained by collisional excitation of Ne-like ions at wavelengths ranging from 46.9 to 60.8 nm [2,6,9]. In the particular case of Ar discharges the gain-length product for the $3p\ ^1S_0$-$3s\ ^1P_1$ transition of Ne-like Ar at 46.9 nm has exceeded saturation [7], allowing for the generation of laser output pulse energies approaching 1 mJ and average powers up to 3.5 mW [10]. Large amplification was also demonstrated in Ne-like Cl at 52.9 nm [9] and in Ne-like S at 60.8 nm [6]. These lasers required the generation of plasma columns with electron densities of the order of $5\times 10^{18}\,\mathrm{cm}^{-3}$ and electron temperatures in the range of 60–80 eV [2,6,7]. Such conditions were achieved utilizing fast current pulses with peak amplitude between 23 and 40 kA [2,6,7,9]. There is interest in the possible extension of this laser pumping scheme to shorter wavelengths. However, this requires the generation of significantly hotter and denser plasma columns [12,13], which in turn demands a substantial scaling of the excitation power density.

Herein we report the generation and study of capillary discharge plasma columns created utilizing discharge powers between one and two orders of magnitude larger than those used in previous experiments with gas-filled capillaries. The plasma columns were generated utilizing current pulses with 10–90 % rise time of about 10 ns and peak amplitude of up to 200 kA. Utilizing this discharge, Ar plasma columns were generated in capillaries with diameters of 3.3 mm and 4 mm made of either alumina (Al_2O_3) or polyacethal $(CH_2O)_n$ filled with 1.3 T of Ar gas. As discussed below, the discharges in ceramic capillaries produced plasmas with a slightly higher degree of ionization. Since plasma columns with maximum degree of ionization are of most interest for the development of shorter wavelength discharge-pumped lasers, the majority of the data presented in this paper corresponds to ceramic capillaries. The plasmas were diagnosed using time resolved soft-x-ray spectroscopy and pinhole camera images. The dynamic of the plasma was also studied with numerical simulations. The plasma columns obtained are significantly hotter and denser than those reported in all previous gas-filled capillary experiments [2–6,12,13]. The next sections of the paper discuss the generation of the high-power-density capillary discharge plasma columns and the plasma diagnostic measurements, followed by an interpretation of the results based on model simulations.

II. EXPERIMENTS

Fast current pulses were generated through the capillary load utilizing a new type of pulsed power generator composed of three pulse compression stages. The first two stages consist of a conventional Marx generator and coaxial water capacitor that has the purpose of rapidly charging the third and final pulse compression stage. The eight-stage Marx generator is capable of operating at voltages up to 800 kV. The second compression stage, which consists of a 26 nF coaxial water capacitor, is charged in about 1 μs. In turn this water capacitor is discharged through a self-breakdown spark gap pressurized with SF_6 gas to charge the third and final stage in about 75 ns. This rapid charging avoids breakdown of the water-dielectric, and minimizes the charge leakage to ground

*Email address: rocca@engr.colostate.edu

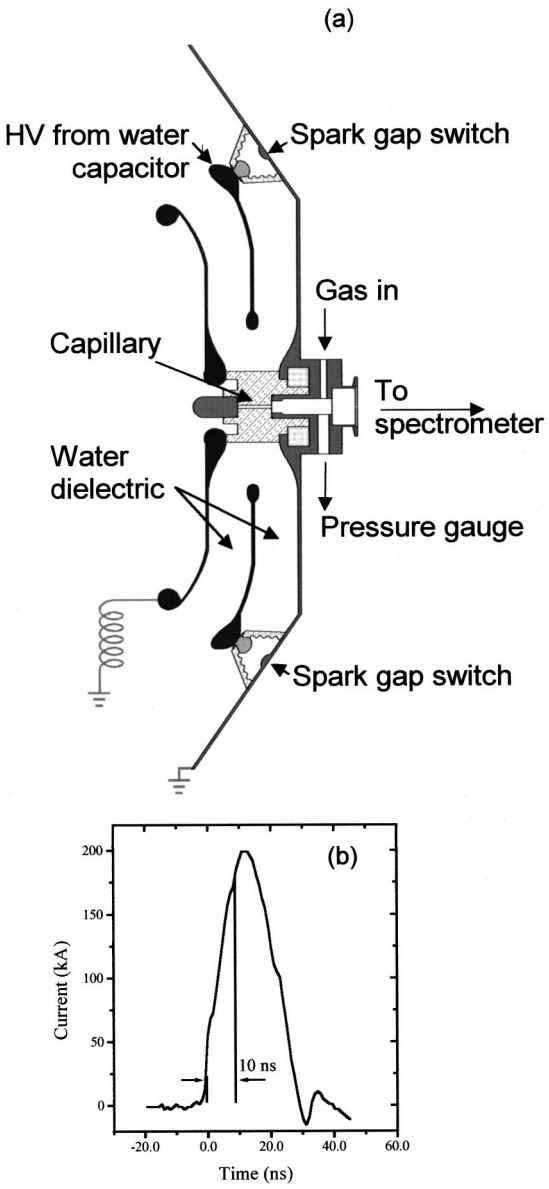

FIG. 1. (a) Schematic representation of the third pulse compression stage, consisting of a radial Blumlein transmission line switched by an array of seven synchronized spark-gap switches. (b) Current pulse.

through the finite resistant of the water used as dielectric in the transmission line of the final compression stages. The third stage, illustrated in Fig. 1(a), is of different design and consists of two radial water dielectric transmission lines connected in a Blumlein configuration. The fast current pulse that excites the capillary plasma is produced by discharging the Blumlein transmission line through an array of seven synchronized triggered spark-gap switches distributed along the outer diameter of the water transmission line. This circular array of gas pressurized spark gaps approximates a large single multichannel spark gap, allowing for a very rapid switching of the Blumlein. The capillary load is placed in the axis of the Blumlein, which together with the spark gap array defines a very low inductance loop that allows for the generation of very fast current rise times, exceeding 1.5×10^{13} A/s. The ground electrode is designed to have a central hole that allows for the observation of the axially emitted plasma radiation. Figure 1(b) illustrates a current pulse having a peak current of 200 kA and a 10–90 % rise time of ~10 ns. The current pulse was measured with a Rogowsky coil having a response risetime of less than 1 ns. These pulse characteristics significantly exceed those of previous experiments with gas-filled capillary discharges [2,12,13]. Immediately preceding the fast discharge pulse the capillary channels were preionized with a current pulse of 20–40 A and 10 μs duration. Typically several tens of shots were made with each capillary. The gas was injected utilizing a pulsed valve and was evacuated through a differential pumping system that made use of two turbomolecular pumps.

The radial evolution of the plasma columns was studied by means of an on-axis pinhole camera. A 90 μm pinhole was utilized to image the plasma over the detection plane with a magnification of 3.5×. The gated detection system, consisting of a microchannel plate (MCP) intensified charge coupled device (CCD) array detector, had a time resolution of ~4 ns. Wavelength discrimination was achieved utilizing one of two different sets of filters in front of the pinhole camera. Figure 2 shows a sequence of time resolved pinhole images of the soft-x-ray emitting region of the plasma for wavelengths mainly below 3 nm. The images correspond to a 4 mm diameter ceramic capillary excited by current pulses of about 190 kA peak current. Wavelength discrimination was obtained using a stack composed of a 1 μm thick carbon filter and a 0.2 μm thick aluminum filter. The carbon filter alone transmits photons below 3 nm, and also in a window between about 4.5 and 10 nm. The addition of the Al filter decreases the transmissivity in this window by a factor that increases from about 6× at 4.5 nm to about 600× at 10 nm as compared with the carbon filter alone, significantly enhancing the relative contribution to the images of photons with wavelengths below 3 nm. The sequence of images shows the formation of a strong shock that originates near the capillary walls and evolves to form a compressed plasma column at the center of the capillary. The earliest image, obtained at 20 ns from the beginning of the current pulse, shows a cylindrical shell with an outer diameter of ~800 μm caused by the current distribution determined by electromagnetic field diffusion from the wall toward the axis. The subsequent images show the rapid continuous compression of the plasma column, which reaches a minimum diameter of about 300 μm at ~25 ns after the beginning of the current pulse. Subsequently the plasma column expands, and the intensity of the radiation emitted within this spectral range decreases rapidly. At times after 31 ns the intensity drops below the detection limit. It should be noticed that the asymmetry observed in the wings of the profiles corresponding to the larger diameter images is caused by an imperfect alignment of the pinhole rather than by an asymmetry in the plasma column. Figure 3 shows a series of pinhole images for discharge conditions similar to those of Fig. 2, but obtained utilizing only the 1 μm thick carbon filter. The removal of the aluminum filter changes the range of detected wavelengths significantly enhancing the contribution from

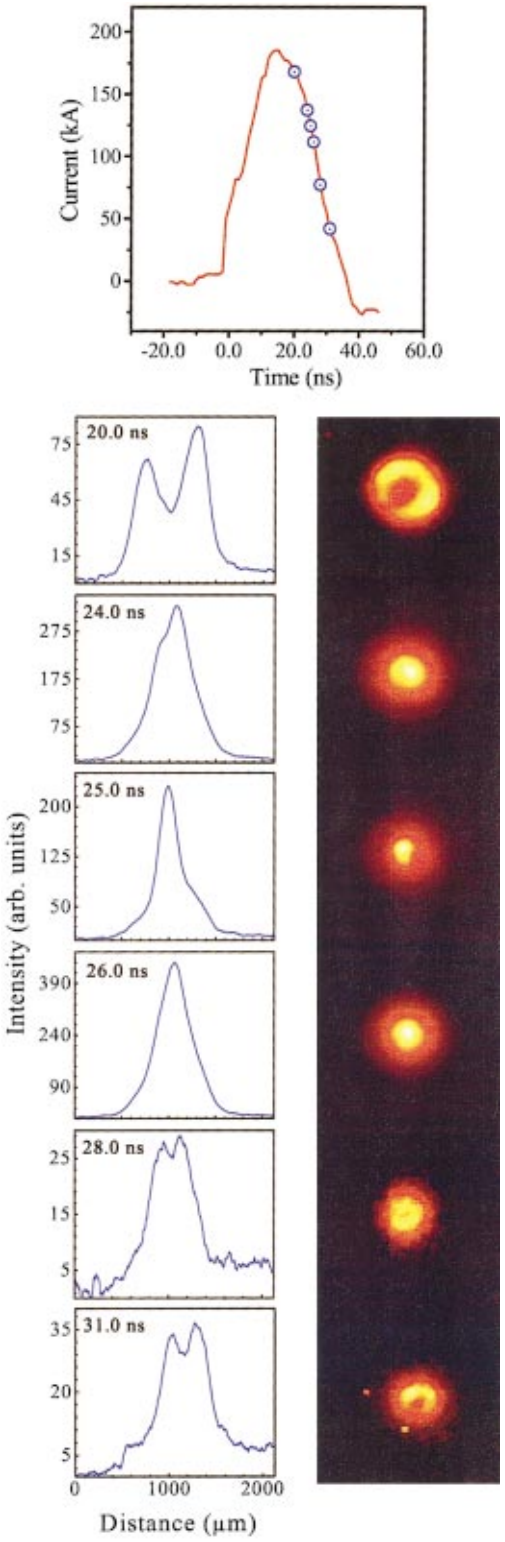

FIG. 2. (Color) Sequence of time resolved pinhole camera images obtained with discharge current pulses of ~190 kA with a 10–90 % rise time of 11 ns through a 4 mm diameter ceramic capillary. The images were taken using a 1 μm thick C filter plus a 0.2 μm thick Al filter. The image corresponds mainly to photons with wavelength below 3 nm.

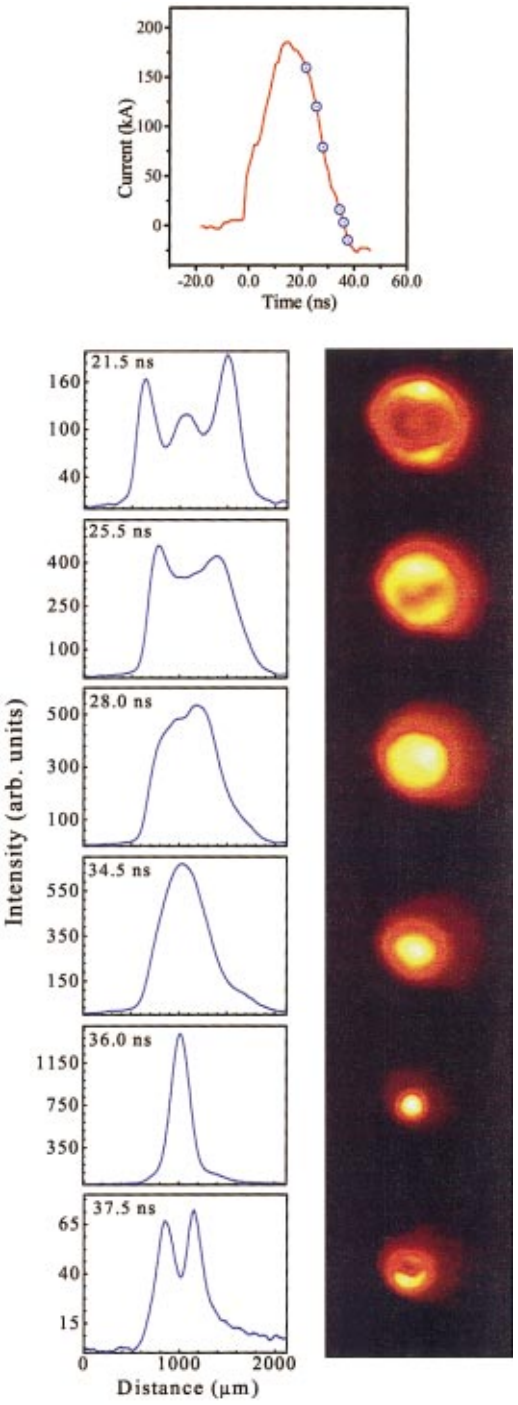

FIG. 3. (Color) Sequence of time resolved pinhole camera images of the plasma for the same discharge conditions of Fig. 2 taken using only a 1 μm thick C filter. The filter transmits photons below 3 nm and also in the range between 4.5 and 10 nm.

photons in the 4.5–10 nm spectral region. In this case the pinch at about 25 ns is largely concealed by the overlap with stronger emission at longer wavelengths, that at this time occurs in a much larger plasma region. However, Fig. 3 clearly shows the occurrence of a latter pinch that takes place around 36 ns from the beginning of the current pulse. This weaker second pinch was not observed with the stack of the two filters and therefore corresponds to a colder plasma. Fig-

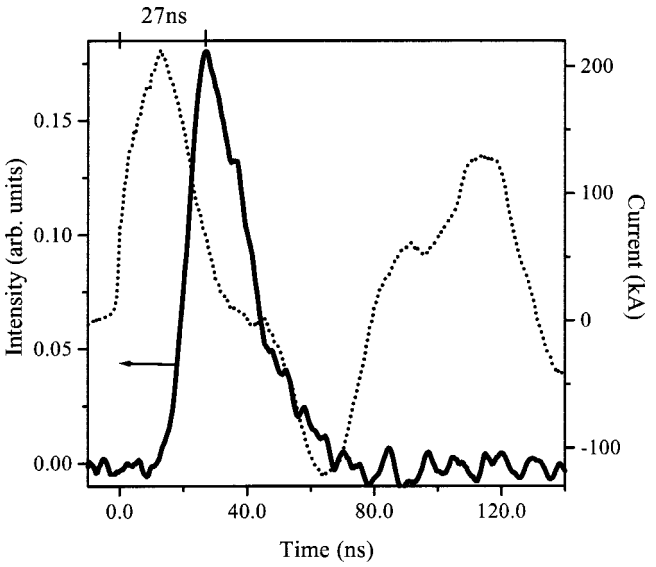

FIG. 4. Correspondence between the evolution current pulse and soft-x-ray emission measured with an MCP intensified vacuum photodiode. The data was obtained using a 1 μm thick C filter plus a 0.2 μm thick Al filter. The image corresponds mainly to photons with wavelength below 3 nm.

ure 4 shows a different measurement of the time evolution of the radiation obtained with an MCP intensified vacuum photodiode and a filter stack composed of a 1 μm thick C filter and a 0.2 μm thick Al filter. This measurement shows that in the 4 mm diameter capillaries the maximum emission occurs $\sim$27 ns after the initiation of the current pulse.

Time resolved spectroscopy was carried out through selected intervals in the spectral range between 3 and 30 nm to study the evolution of the degree of ionization of the plasma. The radiation axially emitted by the plasma was analyzed using a 1 m grazing incidence spectrograph having a 1200 l/mm gold coated grating placed at 85.8°. A cylindrical mirror placed at a grazing incidence angle of 2° was used to collect the radiation and focus it into the entrance slit of the spectrograph. The time resolved spectra were recorded utilizing a gated MCP/CCD detector with a temporal resolution of $\sim$5 ns. The spectral range between 18 and 23 nm, which contains spectral lines belonging to all the ionization stages between Ar XI through Ar XV, was found to be the most suitable to study the time evolution of the plasma. Figures 5(a) and 5(b) show typical spectra corresponding to a time near the occurrence of maximum ionization for polyacethal and ceramic capillaries, respectively. They correspond to plasma columns generated using current pulses with 197 kA peak amplitude and a 10–90 % rise time of 11 ns. The dominance in the ceramic capillaries of the Ar XV line at 22.11 nm (identified with an arrow in the spectra), and the larger intensity ratio between adjacent 18.795 nm Ar XIV and 18.882 nm Ar XI lines visible at the left of the spectra in Fig. 5(b), are indicative of a larger degree of ionization.

The series of time resolved spectra in Figs. 6 and 7 provides information of the temporal variation of the degree of ionization of the plasma for discharges in 4 mm and 3.3 mm diameter ceramic capillaries, respectively. The peak amplitude and rise time of the current pulses were maintained approximately constant for these two series at 190 ± 5 kA and 11.5 ± 1.5 ns (10–90 %), respectively. The variation of the intensity of the Ar XV line relative to the Ar XIV lines and the changing ratio of intensities between the two adjacent lines of Ar XIV and Ar XI at the left of the spectra give again an indication of the variation of the degree of ionization. This line intensity ratio peaks around the time corresponding to the first pinch, identified in the pinhole images in the vicinity of 25 ns. Figure 7 shows that the Ar XV line is almost absent at 18.4 ns after the beginning current pulse and begins to dominate approximately at 21.6 ns after the initiation of the current pulse.

The high intensity of the Ar XV line in the ceramic capillaries suggests that lines corresponding to Ar XVI ions might also be present. Line emission was indeed observed at several wavelengths corresponding to Ar XVI lines in the 3–30 nm range. However, the presence of these lines could not be confirmed due to their overlap with first or second order lines from Ar ions of lesser charge. Nevertheless, the theoretical calculations discussed below predict the existence of Ar XVI ions under the operating conditions of this capillary discharge. These simulations, performed with the code RADEX [10–13], show that in the case of steady-state ionization equilibrium calculated for the average value of the electron density over the time of collapse, the Ar XV ions reach maximum abundance at a temperature of $\sim$160–180 eV. In such ionization equilibrium conditions, slightly larger temperatures $T_e\sim180-200$ eV are required for the relative intensities of Ar XIV and Ar XV lines to be similar to those observed in the experiment. However, the ionization equilibrium values usually represent only an estimate of the lower limit of the real temperature. In the dynamic situation of the experiment, in which the limited hot plasma lifetime is shorter than the ionization time for the high-Z species present in the plasma, the temperature necessary for the creation of such spectra is notably larger. Transient ionization and hydrodynamic calculations done with RADEX, indicate the maximum electron temperature required to generate such spectra must be larger than 250 eV. This suggests the possibility of using fast high current capillary discharges for generating high-temperature plasmas approaching the keV range.

III. MODEL SIMULATIONS

The evolution of the plasma column was modeled with the one-dimensional radiative hydrodynamic-atomic code RADEX [13–15]. The model includes two temperature hydrodynamics equations, Maxwell's equations, and multicomponent atomic kinetics and radiation transport. The physical model remains in most respects similar to the one which was applied to the study of capillary discharge soft-x-ray lasers [7,12–14] and microcapillary plasmas [15] in recent years, but includes the atomic kinetics of the highly ionized species needed to reproduce the experimentally observable characteristics of this much higher power capillary discharge. It also contains a description of wall ablation for either polyacethal or ceramics capillaries, which includes the use of the equations of state for the solid material and the plasma, and

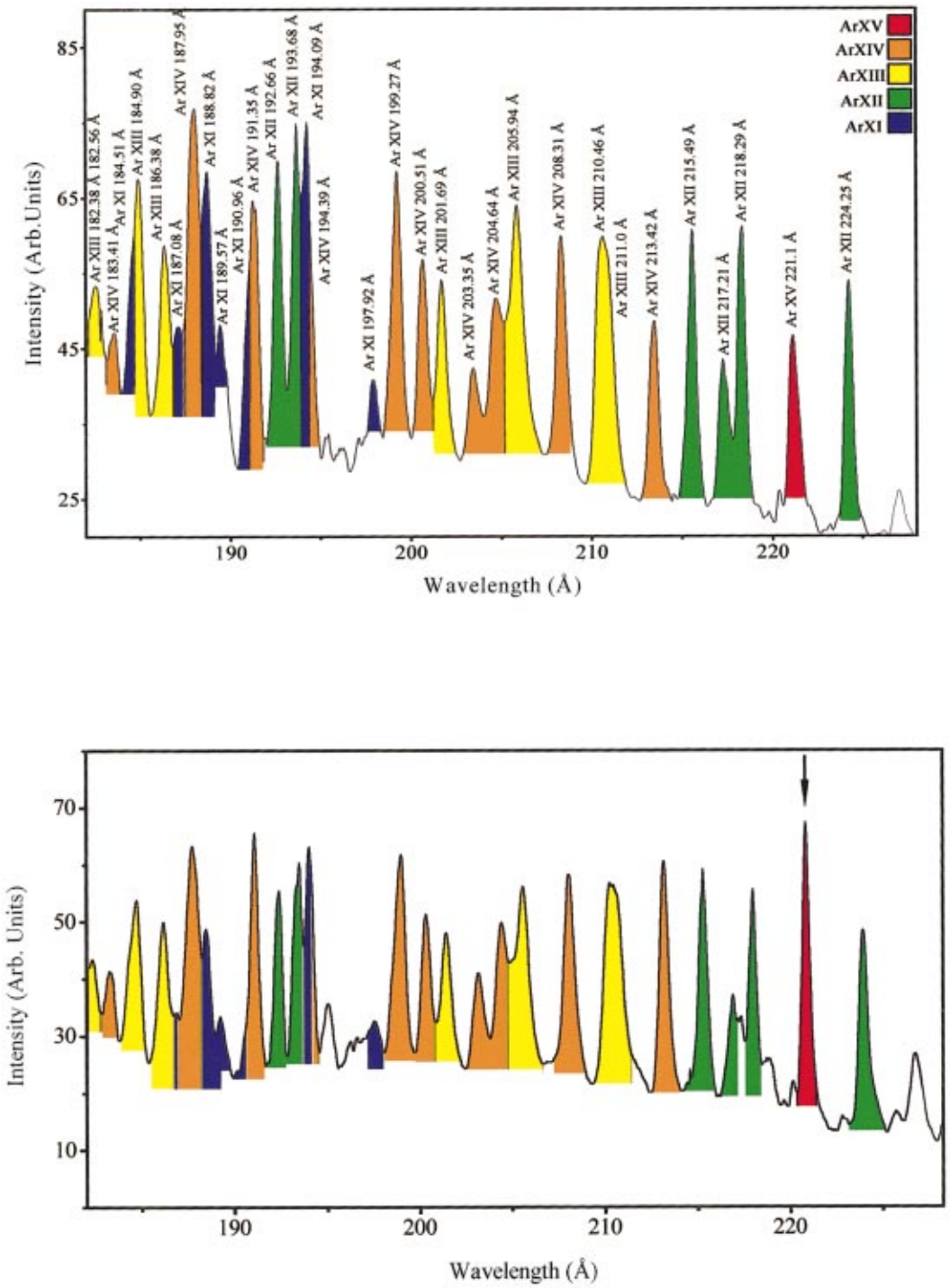

FIG. 5. (Color) Time resolved spectra corresponding to (a) polyacethal capillary, and (b) ceramic capillary obtained at the time of maximum ionization. The peak current was 197 kA with a rise time of 11 ns.

the phenomena of vaporization and ionization to reproduce the phase transformation from solid to vapor and finally to plasma [16,17].

To obtain a consistent picture of the dynamics of the capillary plasma we performed numerous comparisons between the simulations, the experimental spectra, and pinhole images for a large variety of experimental conditions. In the RADEX radiation hydrodynamics the transport of the photons inside the atomic line profiles was modeled in the Biberman-Holstein approximation [18] which takes advantage of the 1D symmetry of the capillary plasma. More than 30 000 lines were included, of which nearly 3000 are observed in the spectral region between 15 and 23 nm. Two-dimensional edge effects associated with the escape of the plasma from the capillary are not important in such short-pulse high-current device, and are negligible for many applications such as soft-x-ray lasers. However, the axial velocity spread at the end of the column somewhat influences the opacity of optical

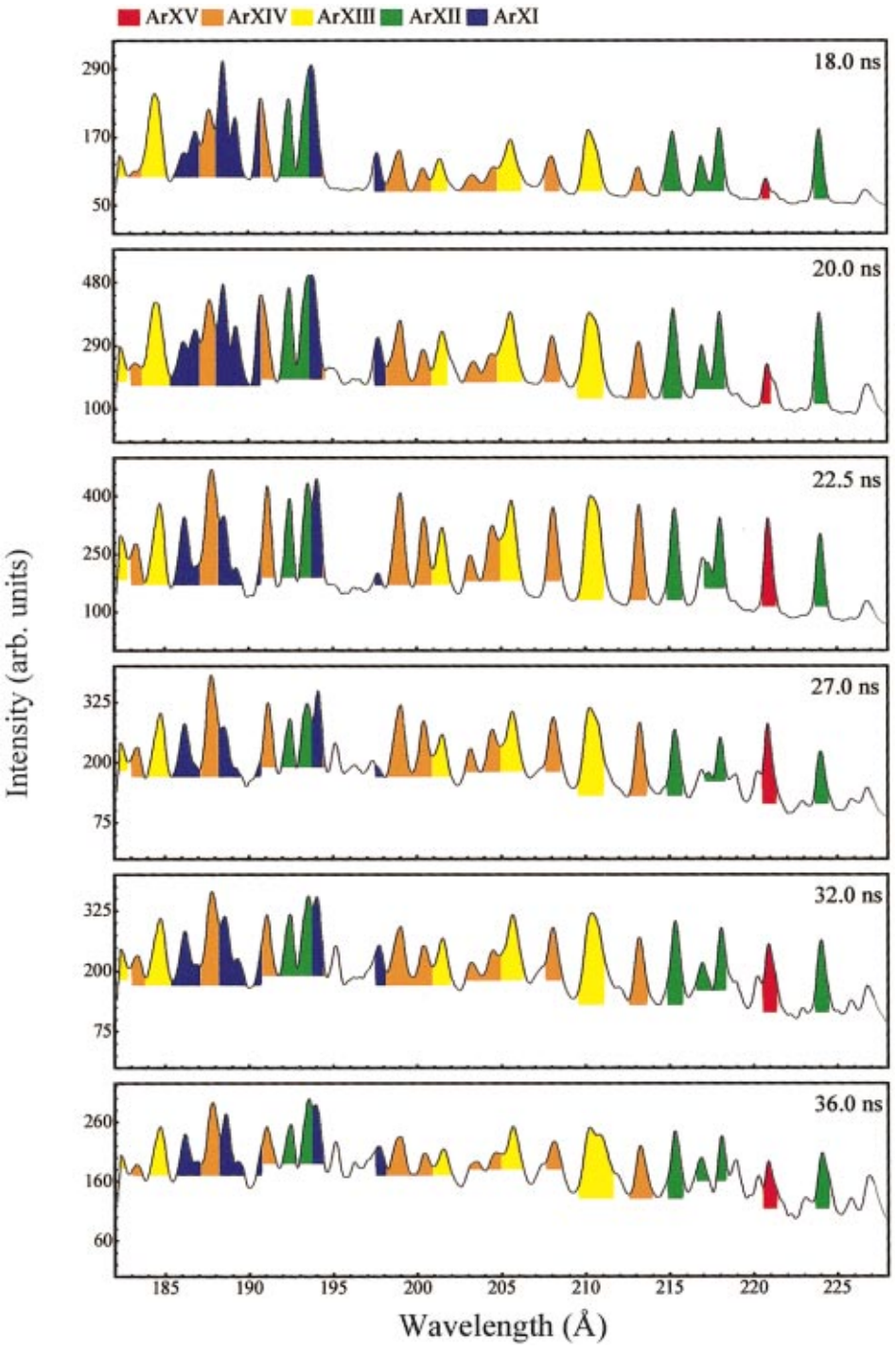

FIG. 6. (Color) Sequence of time resolved spectra corresponding to a 190 ± 5 kA discharges through a 4 mm diameter ceramic capillary. The 10–90 % current rise time was 11.5 ± 1.5 ns.

thick lines emitted from the exit region of the capillary facing the spectrometer. Hence, the synthesized spectra corresponding to these conditions cannot be expected to precisely match the measured spectra. Nevertheless, since the main effect of the radiation on the hydrodynamic and atomic kinetics is dominated by the radiation transport in the radial direction, the computed spectra not only show all the lines identified in the experiments, but also reasonably match their intensities.

Note that a similar range of capillary diameters, gas pressures and composition was previously investigated for smaller current discharges [7,12]. It was found in the calculations that the major difference between the high current and the lower current cases is the much larger shock-induced plasma temperature change, as it is natural to expect from the much larger amplitude and shorter duration of the current pulse. In this case the plasma speed just before the collapse reaches 2×10^7 cm/s as compared to 6×10^6 cm/s in the case of the 40 kA discharges used in the first Ne-like Ar soft-x-ray laser experiments [2,7,12]. The depth of the layer in front of the hot dense shock is of the order of 100–200 μm and is defined by the heat conductivity in the low density gas, and in a lesser extent by the process of electromagnetic field diffusion. The process of heat conduction substantially facili-

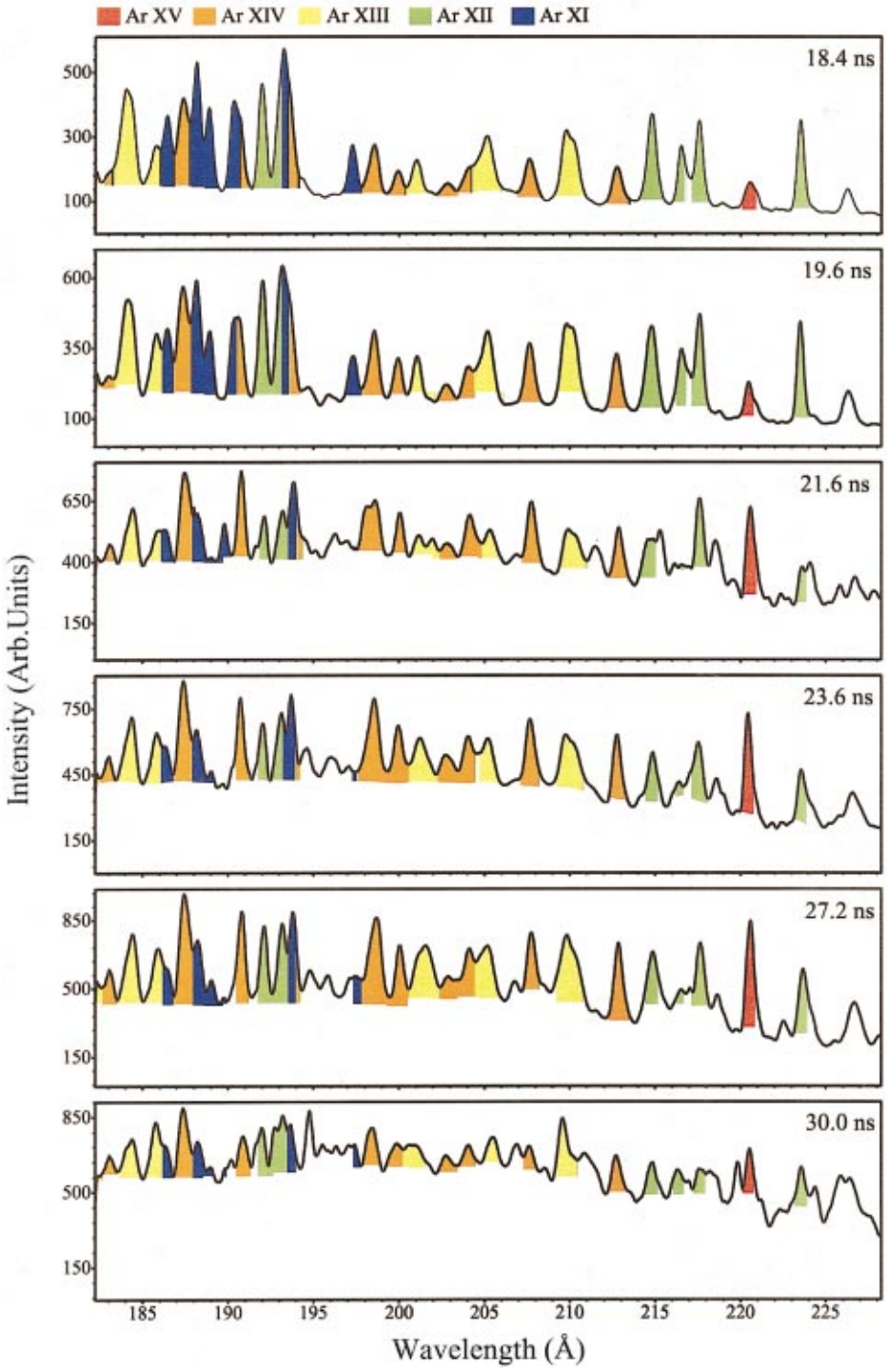

FIG. 7. (Color) Sequence of time resolved spectra corresponding to a 190 ± 5 kA discharges through a 3.3 mm diameter ceramic capillary. The 10–90 % current rise time was 11.5 ± 1.5 ns.

tates the achievement of the high electron temperature resulting in the high degree of ionization observed in the experiment, by introducing additional entropy in the compressed core before the shockwave collapses on axis. Also when the heat wave and the electromagnetic wave arrive on axis, the maximum of the current density and joule dissipation switch to the center of the capillary as in the Ne-like Ar soft-x-ray laser case. Quickly after that, within 1–2 ns, the front of the shock wave arrives to form the hot dense plasma column. Mass continues to be supplied, and after several more ns the plasma starts to cool due to expansion, radiation losses and current decay. At the time of maximum compression the interface between the Ar plasma and the evaporated wall material is computed to be positioned relatively far from the compressed central region, $\sim 250-400$ μm. The total current flowing inside the compressed plasma column is a small fraction of the order of 10–15 % of the total current. As it was noted in Ref. [19], this situation probably helps to suppress the current instabilities. Hence, it is reasonable to suggest that the combination of several factors including the smaller current and pinch radius, together with very good initial plasma symmetry and relatively short time duration of

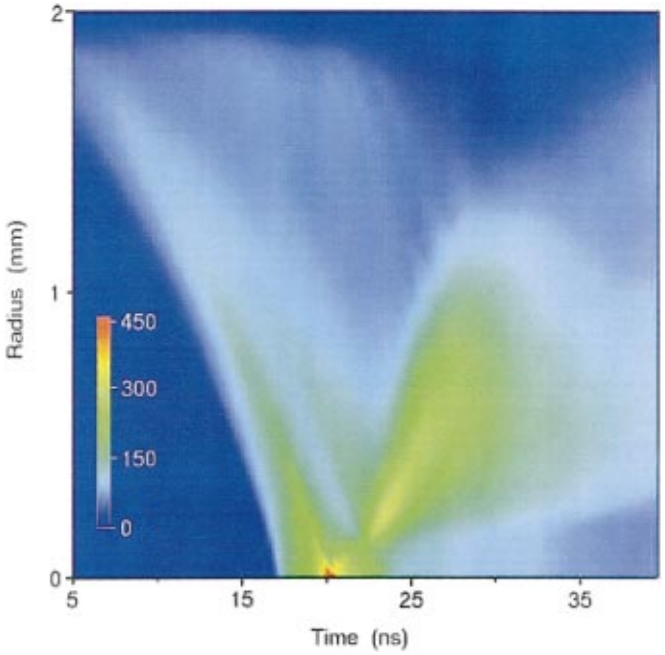

FIG. 8. (Color) Computed spatiotemporal evolution of the electron temperature in a 4 mm diameter ceramic capillary filled with 1.3 T of Ar excited by a 195 kA current pulse. The color scale shows electron temperatures in eV.

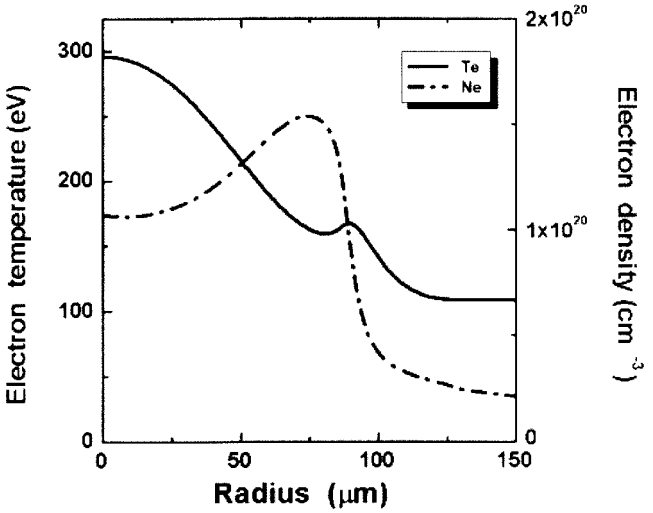

FIG. 9. Computed electron temperature and electron density profiles near the time of maximum compression for a discharge through an argon filled ceramic capillary of 3.3 mm diameter. The rest of the discharge conditions are equal to those of Fig. 8.

the entire compression process, substantially facilitate the suppression of the MHD and current instabilities which commonly plague most high current discharge experiments. However, further 2D and 3D numerical modeling is required to determine the main reason of the relatively good stability of these discharges.

The shock wave originates in the vicinity of the capillary surface as the result of the strong ponderomotive $\mathbf{J}\times\mathbf{B}$ force and heating in the skin layer, and then propagates with the speed defined by electromagnetic field diffusion, the Alfven time, and hydrodynamics time. The plasma compression on axis and the dissipative electron viscous heating [20] are computed to induce for a brief period of time a maximum electron temperature as high as 450–500 eV. However, as shown in Fig. 8, this temperature rapidly relaxes to 200–270 eV in 1–2 ns due to strong ionization and line radiation at electron densities of $(1-2)\times10^{20}\,\mathrm{cm}^{-3}$, which are 3–4 times higher than those obtained in the case of the 40 kA capillary discharges. The electron density reaches its maximum value 3–5 ns after the time of maximum temperature, which corresponds to the minimum observable source size. The nonstationary degree of ionization also reaches its maximum average ion charge of $Z_s\sim15.4$ at this time, and 3–4 ns later the plasma starts to recombine. Figure 9 shows the computed radial profile of the electron temperature and density at the time of maximum compression for the 3.3 mm diameter ceramic capillary with the same discharge conditions as in Fig. 8. The calculated electron temperature and density on axis are 295 eV and $1.2\times10^{20}\,\mathrm{cm}^{-3}$, respectively.

The compressed plasma diameter is computed to reach a minimum diameter of 250–300 μm at ~19 ns and ~25 ns after the initiation of the current pulse in the 3.3 mm and 4 mm diameter capillaries, respectively. This size of the soft-x-ray emitting is in agreement with the observed extent of the soft-x-ray emitting region of the plasma at the time of maximum compression. The simulations also show that a concave electron density profile is formed in the axial region by the reflected shock ~1.5 ns after the column collapse. This prediction is corroborated by the observation of a depression at the axis of the soft-x-ray emission profiles in the pinhole image acquired a few ns after the maximum compression (see the 28 ns and 31 ns frames in Fig. 2). Such kind of electron density profile might be advantageous for some applications, for example waveguiding of soft-x-ray laser beams. Note that, as in previous soft-x-ray laser experiments, in the current experimental setup the time of the plasma column collapse is well matched to the current pulse duration. Hence the energy stored in the driving circuit is well utilized, resulting in efficient plasma generation.

The amount of mass ablated from the capillary wall and involved into the plasma compression process is smaller for the ceramic capillaries than for those made of polyacethal. This is due to several factors, among which are the larger activation energy and thermal conductivity of alumina relative to that of easily thermally decomposed plastic. However, the hydrodynamics of plastic and ceramics wall capillaries were not found to be greatly different. The moment of arrival of the shock wave to the center is similar, 17 and 17.5 ns, respectively, since it is mostly defined by the ponderomotive force and thermal pressure exerted on the plasma in the initial ~10 ns of the discharge, when the evaporated part of the total mass is very small. In both cases, quickly after the initial stage of the discharge, an additional acceleration of the shock front due to electromagnetic field diffusion takes place in the argon part of the plasma column. This acceleration further minimizes the differences in compression time. The electron temperature is slightly larger in the case of the ceramics capillary, resulting in the more intense Ar XV line emission observed in the experiments. This is mainly the

result of higher plasma heating arising from the nearly two times larger plasma resistivity in the case of the higher Z ceramic capillary plasma [21]. The differences in resistivity do not have a major effect on the overall discharge current, because it is mainly defined by the larger impedance of the generator.

IV. CONCLUSIONS

In summary, we have generated plasma columns of about 300 μm diameter and electron temperatures >250 eV utilizing fast discharge pulses with a current rise time of $\sim 1.5 \times 10^{13}$ A/s and peak currents up to 200 kA. Model computations predict plasma column diameter and spectra similar to those observed in the experiments, and suggest the electron densities reach values $>1\times 10^{20}\,\mathrm{cm}^{-3}$. These plasma conditions fulfill the requirements necessary for a variety of possible applications, in particular for attempting the demonstration of discharge-pumped lasers at significantly shorter wavelengths. Of main interest are laser transitions in Ni-like ions, sequence which scales to shorter wavelengths more rapidly than the Ne-like sequence used in the previous capillary discharge soft-x-ray laser demonstrations. For the high electron temperatures and densities that the above results show are achievable with these type of high current capillary discharges, the atomic elements suitable for lasing in the Ni-like sequence range from $Z=42$ (Mo) to 50 (Sn). The wavelengths of the $4d\ ^1S_0$-$4p\ ^1P_1$ transition of these elements cover the region between 18.9 and 11.9 nm. For example, for the 13.2 nm line of Ni-like Cd XXI the gain is calculated to be ~ 1–$2\ \mathrm{cm}^{-1}$, and potentially $>3\ \mathrm{cm}^{-1}$ for optimum discharge parameters. Larger gain coefficients are estimated for Ni-like Ag XX (13.9 nm) and Pd XIX (14.65 nm).

ACKNOWLEDGMENTS

This work was supported by DARPA Grant No. DAAD 19-99-1-0279 and by the National Science Foundation Grant No. ECS-9713297. Part of the work of V.N.S. and A.L.O. was performed under the auspices of the US Department of Energy at the University of California Lawrence Livermore National Laboratory. The support of the W.M. Keck Foundation to Colorado State University is also gratefully acknowledged.

[1] J. J. Rocca, Rev. Sci. Instrum. **70**, 3799 (1999).
[2] J. J. Rocca, V. N. Shlyaptsev, F. G. Tomasel, O. D. Cortazar, D. Hartshorn, and J. L. A. Chilla, Phys. Rev. Lett. **73**, 2192 (1994).
[3] B. E. Lemoff, G. Y. Yin, C. L. Gordon III, C. P. J. Barty, and S. E. Harris, Phys. Rev. Lett. **74**, 1574 (1995).
[4] D. Korobkin, C. H. Nam, S. Suckewer, and A. Golstov, Phys. Rev. Lett. **77**, 5206 (1996); D. Korobkin, *et al.*, *ibid.* **77**, 1476 (1996).
[5] P. V. Nickles, V. N. Shlyaptsev, M. Kalashnikov, M. Schnurer, I. Will, and W. Sadner, Phys. Rev. Lett. **78**, 2748 (1997).
[6] F. G. Tomasel, J. J. Rocca, V. N. Shlyaptsev, and C. D. Machietto, Phys. Rev. A **55**, 1437 (1996).
[7] J. J. Rocca, D. P. Clark, J. L. A. Chilla, and V. N. Shlyaptsev, Phys. Rev. Lett. **77**, 1476 (1996).
[8] J. Dunn, A. L. Osterheld, S. Sheperd, W. E. White, V. N. Shlyaptsev, and R. E. Stewards, Phys. Rev. Lett. **80**, 2825 (1998).
[9] M. Frati, M. Seminario, and J. J. Rocca, Opt. Lett. **25**, 1022 (2000).
[10] C. D. Machietto, B. R. Benware, and J. J. Rocca, Opt. Lett. **24**, 115 (1999).
[11] J. J. Rocca, O. D. Cortazar, B. Szapiro, K. Floyd, and F. G. Tomasel, Phys. Rev. E **47**, 1299 (1993).
[12] J. J. Rocca, F. G. Tomasel, M. C. Marcc DAAD 19-99-1-0279
L. A. Chilla, B. T. Szapiro, and G. Giu
2547 (1995).
[13] V. N. Shlyaptsev, A. V. Gerusov, A. V. V
O. D. Cortazar, F. Tomasel, and B. Sza
99 (1993).
[14] V. N. Shlyaptsev, J. J. Rocca, and A. L.
2520, 365 (1995).
[15] M. Marconi, C. Moreno, J. J. Rocca, V. N. Shlyaptsev, and A. Osterheld, Phys. Rev. E **62**, 7209 (2000).
[16] Yu. V. Afanasiev and O. N. Krokhin, *High Temperature Plasma Phenomena Under the Influence of High Power Radiation with Matter* (Mir, Moscow, 1974) (in Russian).
[17] A. A. Samokhin, in *Proceedings of the Geberal Physics Institute* (Nauka, Moscow, 1998), Vol. 13 (in Russian).
[18] L. M. Biberman, Sov. Phys. JETP **17** 416 (1947); T. Holstein, Phys. Rev. **72**, 1212 (1947); **83** 1159 (1951).
[19] N. A. Bobrova, S. V. Bulanov, T. L. Razinkova, and P. V. Sasorov, Plasma Phys. Rep. **22**, 349 (1996).
[20] K. G. Whitney, Phys. Plasmas **6**, 816 (1999).
[21] L. Spitzer, *Physics of Fully Ionized Gases* (Wiley, New York, 1957); S. I. Braginskii, in *Transport Processes in Plasmas*, edited by M. A. Leontovich (Consultants Bureau, New York, 1963), p. 205.

Physica Scripta. Vol. 67, 414–419, 2003

Identification of $n = 4$, $\Delta n = 0$ Transitions in the Spectra of Nickel-like Cadmium Ions from a Capillary Discharge Plasma Column

A. Rahman[1], E. C. Hammarsten[1], S. Sakadzic[1], J. J. Rocca[1,*] and J.-F. Wyart[2,**]

[1] Electrical and Computer Engineering Department, Colorado State University, Fort Collins, CO 80523, USA
[2] Laboratoire Aime Cotton, CNRS (UPR 3321), Centre Universitaire, 91405-Orsay, France

Received December 11, 2002; accepted December 27, 2002

PACS ref: 32.30, 32.70, 42.55.

Abstract

Spectra of Nickel-like Cadmium (CdXXI) ions in the 12.7–18.4 nm wavelength region obtained with a high current capillary discharge have been analyzed. Fifty-three $3d^9\,4p$–$3d^9\,4d$ and $3d^9\,4d$–$3d^9\,4f$ CdXXI lines were identified with the assistance of calculations performed using the Slater–Condon method with generalized least-squares fits of the energy parameters. The average deviation between the measured and theoretical wavelengths is $\langle \lambda\,\mathrm{exp} - \lambda\,\mathrm{th} \rangle = 0.0065$ nm. The results demonstrate that fast capillary discharges can produce high quality spectra for the study of multiply charged ions with charges of up to at least $Z = 20$.

1. Introduction

There is significant interest in the spectra of Ni-like ions in relation to the development of soft X-ray lasers [1–4]. Of particular interest is the spectrum of Ni-like cadmium in relation to the development of efficient lasers for metrology applications in the vicinity of 13.5 nm, the wavelength that has been selected for the nanolithography to be used in the future generations of integrated circuits. Laser amplification can be obtained at 13.2 nm by creating a population inversion between the $3d^9\,4d\,^1S_0$–$3d^9\,4p\,^1P_1$ levels of Ni-like CdXXI [2].

Several previous works have studied the energy level structure and oscillator strengths of Ni-like Cd ions. Transitions to the ground state $3d^{10}$ were observed at low resolution in [5] and surveyed theoretically by MCDF [6], parametric potential [7] and RMBPT methods [8]. At wavelengths longer than 13.2 nm, non-lasing lines have been observed from laser produced plasmas (LPP). However, the twenty-one lines published in [9] left numerous $3d^9 4d$–$3d^9 4p$ and all $3d^9 4d$–$3d^9 4f$ transitions to be identified. Theoretical investigations of 4-4 transitions in [8] were limited to s-p and (partly) p-d transitions. In this work we report the identification of 53 transitions corresponding to Ni-like Cd ions based on spectra obtained from cadmium plasma columns generated using a fast capillary discharge. The spectroscopy of ions with such a high degree of ionization in discharge-created plasmas is made possible by a new type of fast capillary discharge that operates at peak currents of up to 200 kA and current risetimes exceeding 1.5×10^{13} A/s [10]. Relative to laser-created plasmas these capillary discharge plasmas have a lower electron density. Consequently, the spectra of these capillary discharge plasmas are clearly dominated by lines and often present a very small continuum background, which constitutes an advantage for the identification of spectral lines.

The next section discusses the plasma generation technique used as well as the spectroscopic tools used to acquire and calibrate the spectra. The theoretical computation used for interpretation of the spectra and for the line assignment is described in Section 3.

2. Plasma generation set-up and spectrometer calibration

The Cd plasmas were generated by exciting capillary channels filled with Cd vapor using a high power density pulse generator [11] that produces current pulses with a peak amplitude of up to 200 kA and a 10–90% rise time of 10–15 ns. Utilizing this discharge, Cd plasma columns were generated in polyacethal $(CH_2O)_n$ capillaries with diameters of 5 mm. The pulsed power generator consists of three pulse compression stages. The first two stages consist of a conventional Marx generator and 26 nF coaxial water-dielectric capacitor that has the purpose of rapidly charging the third and final pulse compression stage. The eight-stage Marx generator was operated at an erected voltage of $\sim$650kV. The second compression stage is charged in about 1 μs. In turn this water capacitor is discharged through a self-breakdown spark gap pressurized with SF_6 gas to charge the third and final stage in about 75 ns. The third stage consists of two radial water dielectric transmission lines connected in a Blumlein configuration. The fast current pulse that excites the capillary plasma is produced by discharging the Blumlein transmission line through an array of seven synchronized triggered spark-gap switches distributed along the outer diameter of the water transmission line. This circular array of gas pressurized spark-gaps approximates a large single multi-channel spark gap, allowing for a very rapid switching of the Blumlein. The capillary load is placed in the axis of the Blumlein, which together with the spark gap array defines a very low inductance loop that allows for the generation of very fast current risetimes, exceeding 1.5×10^{13} A/s. The ground electrode is designed to have a central hole that allows for the observation of the axially emitted plasma radiation. The current pulse corresponding to each discharge shot was measured with a Rogowsky coil having a response risetime of less than 1 ns. Cd vapor was injected into the capillary through the hollow anode electrode of the capillary discharge. The Cd vapor was produced by a metal vapor gun designed to generate Cd vapor in a room temperature environment by rapidly

* Rocca@engr.colostate.edu
** Francois.Wyart@lac.u-psud.fr

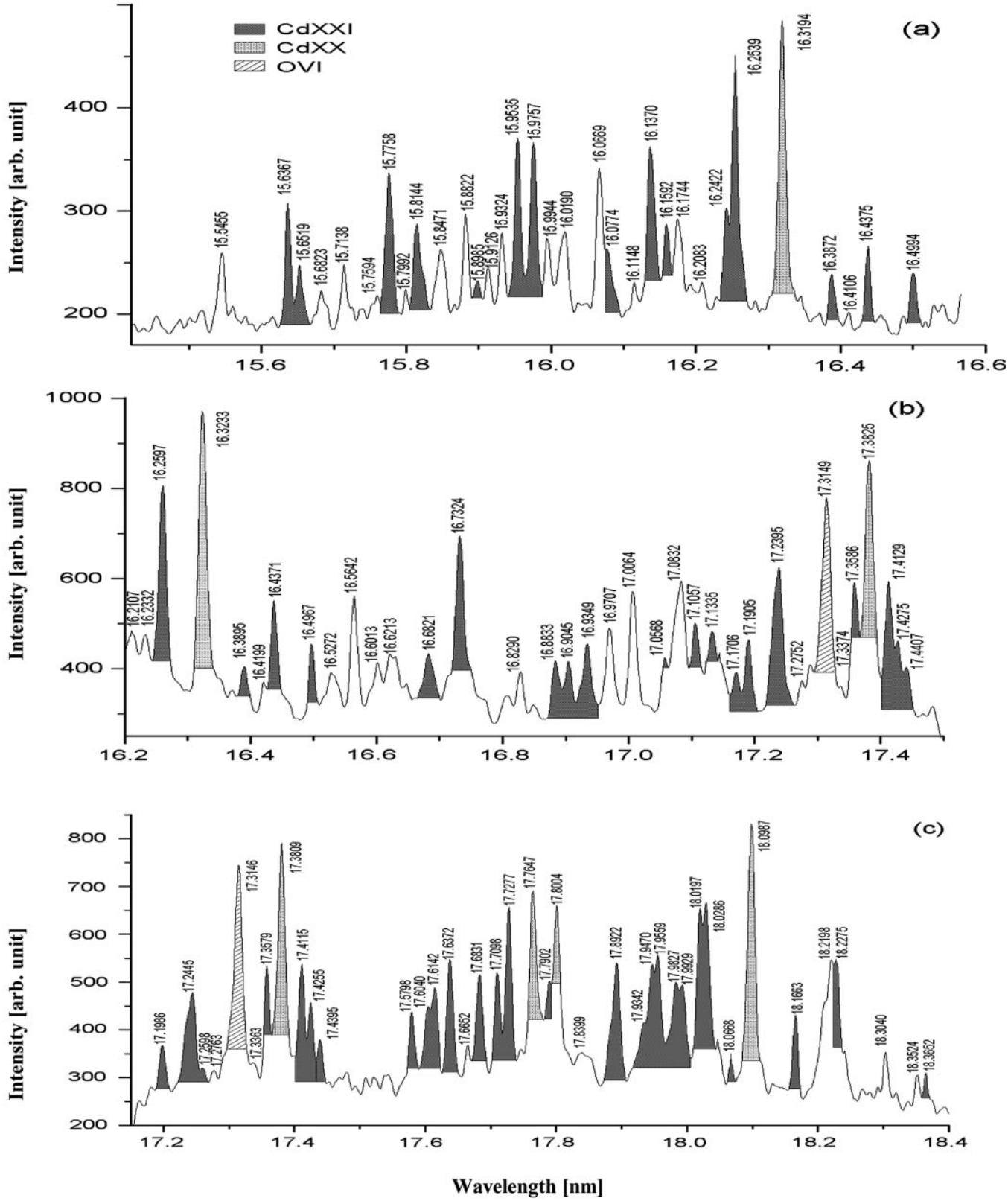

Fig. 1. (a–c) Spectra of a cadmium capillary discharge plasma column for the 15.4–18.4 nm wavelength region. Each spectrum corresponds to a single discharge pulse and was acquired with time resolution of 5 ns at 31.5, 34, and 40 ns after the initiation of the current pulse respectively. The current had peak amplitudes of 178, 188, and 182 kA respectively. The capillary diameter was 5 mm. Each spectral line is identified with the experimental wavelength resulting for the calibration corresponding to that particular shot. The difference in the wavelength of the lines appearing in the overlapping regions are illustrative of the error associated with the measurements. Some of the experimental wavelengths of the lines listed in table III are averages of two or more spectra.

heating a cadmium electrode with a capacitive discharge. Following its injection into the capillary channel, the Cd vapor was pre-ionized with a low current pulse preceding the fast high current pulse. Typically several tens of shots were made with each capillary. Observation of the plasma columns with a soft X-ray pinhole camera shows the current pulse rapidly compresses the plasma to form a hot and dense plasma at the capillary axis. A cylindrical shock

Table I. *Characteristics of the presently available theoretical studies by means of generalized least-squares (GLS) fits for $3d^9 4l$ configurations with the number of different ions N_{ions}, total number of levels N_{lev} and of adjustable parameters N_{par}, the average of deviations, and the gain in N_{lev}/N_{par} ratio in comparing individual and generalized least-squares.*

Config	N_{ions}	N_{lev}	N_{par}	$\langle \Delta E \rangle$ (cm^{-1})	$N_{\text{lev}}/N_{\text{par}}$ *ILS*	$N_{\text{lev}}/N_{\text{par}}$ GLS
$3d^9 4s$	19	75	26	10	1.3	2.9
$3d^9 4p$	23	233	41	46	1.5	5.7
$3d^9 4d$	21	228	38	95	2	6
$3d^9 4f$	19	171	31	140	2.2	5.5

wave shell is driven towards the axis of the discharge by the Lorentz force and by large thermal pressure gradients that arise near the capillary wall [11]. Pinhole camera measurements show the onset of significant soft X-ray emission occurs about 27 ns after the initiation of the current pulse, with rapidly increasing intensity in the few ns after that. The diameter of the soft X-ray emitting regions decreases as the plasma column compresses, until it achieves a minimum diameter of 250–350 μm at 32–34 ns after the onset of the current. Shortly afterwards the emitted soft X-ray intensity rapidly decreases.

The radiation axially emitted by the plasma was focused by a gold-coated grazing-incidence mirror into the slit of a 2.217 m grazing-incidence spectrograph. The spectrograph contained a 2400 lines per millimeter gold-coated diffraction grating mounted at an angle of incidence of 85.8 degrees. The detector consisted of a stack of two microchannelplates (MCP) in chevron configuration, a phosphor screen, and a CCD detector array. The CCD consisted of a front illuminated array of 1024 by 1024 pixels of 24 μm size that was thermoelectrically cooled. All the spectra have a temporal resolution of about 5 ns obtained by gating the MCPs with a voltage pulse. Time resolved spectroscopy was carried out through selected intervals in the spectral range between 10 and 20 nm. The spectral calibration was performed utilizing the wavelengths of known ionic transitions from capillary wall ablated material and from selected gases injected into the capillary channel. The spectral region between 12.7 nm and 13.6 nm was calibrated with lines of FVII, ArVIII, OVI and OVII [12]. The spectral region expanding from 15.4 nm to 18.4 nm was calibrated using numerous transitions of Ar ions corresponding to different stages of ionization ranging from ArX to ArXIV [12]. An indication of the error involved in the calibrations was obtained through a comparison with published wavelength of four CdXX lines [13–15]. All the presently observed CdXX lines were within 0.004 nm of the published values. From these results, from a similar comparison for OVI lines, and from the shot to shot variations of the measured wavelengths, the error in the measured transition wavelengths we are reporting can be conservatively estimated at 0.01 nm.

Table II. *Energy levels of CdXXI. Levels are designated in (J1, j2) coupling scheme, with* J *and* N *index numbering from the lowest level in its* J*-value for the configuration. The (J1, j2) purity in % is followed by SL leading components and purities. The experimental energies are from [9] for $3d^9 4s$ and $3d^9 4p$ and from the present work for $3d^9 4d$ and $3d^9 4f$. E_{GLS} are from the present work. Values are in cm^{-1}.*

Config.	Multiplet	*J*	*N*th	%	SL %	E_{exp}	E_{GLS}
$3d^{10}$	^{1}S	0	1			0	0
$3d^9 4s$	(5/2,1/2)	3	1	100	^{3}D 100	3059268	3059362
	(5/2,1/2)	2	1	99	^{3}D 51	3066123	3066109
	(3/2,1/2)	1	1	100	^{3}D 100	3116960	3116938
	(3/2,1/2)	2	2	99	^{1}D 51	3122430	3122466
$3d^9 4p$	(5/2,1/2)	2	1	96	^{3}P 67	3389332	3389541
	(5/2,1/2)	3	1	99	^{3}F 50	3396397	3396372
	(3/2,1/2)	2	2	94	^{3}F 85	3448887	3448903
	(3/2,1/2)	1	1	74	^{3}P 58	3456137	3455958
	(5/2,3/2)	4	1	100	^{3}F 100	3467062	3467084
	(5/2,3/2)	2	3	91	^{1}D 62	3477956	3477946
	(5/2,3/2)	1	2	73	^{1}P 82	3482340	3482343
	(5/2,3/2)	3	2	99	^{3}D 74	3486540	3486478
	(3/2,3/2)	0	1	100	^{3}P 100	3511162	3511163
	(3/2,3/2)	3	3	100	^{3}F 49	3530843	3530922
	(3/2,3/2)	1	3	92	^{3}D 59	3533498	3533337
	(3/2,3/2)	2	4	99	^{3}D 57	3541520	3541628
$3d^9 4d$	(5/2,3/2)	1	1	71	^{3}S 78	3986980	3987347
	(5/2,3/2)	4	1	98	^{3}G 57	4011530	4011763
	(5/2,3/2)	2	1	89	^{3}P 48	4015240	4015035
	(5/2,3/2)	3	1	90	^{3}D 42	4023220	4022741
	(5/2,5/2)	1	2	72	^{1}P 51	4021200	4020881
	(5/2,5/2)	5	1	100	^{3}G 100	4021720	4021807
	(5/2,5/2)	3	2	89	^{3}D 44	4035150	4035181
	(5/2,5/2)	2	2	85	^{1}D 41	4040060	4040192
	(5/2,5/2)	4	2	98	^{3}F 79	4041400	4041522
	(5/2,5/2)	0	1	51	^{3}P 99	4047700	4047797
	(3/2,3/2)	1	3	71	^{1}P 48	4064580	4064639
	(3/2,3/2)	3	3	94	^{3}G 75	4068540	4068039
	(3/2,3/2)	2	3	99	^{3}F 64	4088350	4088228
	(3/2,3/2)	0	2	51	^{1}S 99	4241750	4241992
	(3/2,5/2)	1	4	71	^{3}D 52	4078130	4077736
	(3/2,5/2)	4	3	98	^{1}G 41	4085780	4086008
	(3/2,5/2)	2	4	97	^{3}D 43	4092000	4092296
	(3/2,5/2)	3	4	97	^{3}F 53	4098500	4098302
$3d^9 4f$	(5/2,5/2)	0	1	100	^{3}P 100		4566753
	(5/2,5/2)	1	1	79	^{3}P 89		4572294
	(5/2,5/2)	5	1	97	^{3}H 55	4587620	4587649
	(5/2,5/2)	2	1	74	^{3}P 63		4581343
	(5/2,5/2)	3	1	51	^{3}D 53	4597000	4597387
	(5/2,5/2)	4	1	64	^{3}F 75	4603200	4601625
	(5/2,7/2)	2	2	70	^{1}D 40		4596250
	(5/2,7/2)	6	1	100	^{3}H 100	4585810	4585548
	(5/2,7/2)	4	2	62	^{1}G 48	4603880	4603935
	(5/2,7/2)	5	2	96	^{3}G 76	4606060	4606237
	(5/2,7/2)	3	2	50	^{1}F 49	4608720	4608621
	(5/2,7/2)	1	2	51	^{3}D 85		4617234
	(3/2,7/2)	2	3	86	^{3}D 36		4641317
	(3/2,7/2)	4	3	93	^{3}H 73	4648520	4647106
	(3/2,7/2)	5	3	98	^{1}H 39	4651300	4651369
	(3/2,7/2)	3	4	99	^{3}G 63	4667900	4667627
	(3/2,5/2)	2	4	90	^{3}F 63		4655651
	(3/2,5/2)	3	3	98	^{3}F 41	4660660	4660602
	(3/2,5/2)	4	4	96	^{3}G 46	4666370	4666127
	(3/2,5/2)	1	3	67	^{1}P 93		4725764

3. Interpretation of the energy levels of CdXXI

The first excited configurations $3d^9 nl$ of Ni-like ions have been studied by means of the chain of programs of L.A.C. [16] in the Slater–Racah approach, as described by Cowan [17]. In this perturbative method, a number N_P of radial

Table III. *Classification of lines of Nickel-like CdXXI. The first column shows the calculated wavelengths (λ_{cal} in nm) as they are derived from the "best" experimental level values in Table II, the second and third columns show the experimental wavelengths (λ_{exp}) and wavenumber. Int is the measured relative intensity. The level designations imply the* J*-value and index* N_{th}*, which numbers the levels from the lowest energy in the same* J*-values and configuration, as used in [9]. The emission transition probability* gA *(in* $10^{10}\ s^{-1}$*) in length form is derived by means of Cowan codes for* E_{GLS} *level values with no C.I. effects included.*

λ_{cal} (nm)	λ_{exp} (nm)	σ (cm^{-1})	Int	$\lambda_{exp} - \lambda_{cal}$ (nm)	Jo *N*th		Je *N*th	E_{odd}		E_{even}	*gA*	Comment
12.7289	12.7349	785244		0.0060	4p 1 1		4d 0 2	3456137		4241750	21	
13.1681	13.1618	759774	4	−0.0063	4p 1 2	–	4d 0 2	3482340	–	4241750	164	
15.6381	15.6367	639521	4	−0.0014	4p 2 2	–	4d 2 3	3448887	–	4088350	219	
15.6555	15.6519	638900	2	−0.0036	4p 3 1	–	4d 3 2	3396397	–	4035150	39	
15.7757	15.7758	633882	5	0.0001	4p 2 1	–	4d 3 1	3389332	–	4023220	266	
15.8175	15.8144	632335	3w	−0.0031	4p 1 1	–	4d 2 3	3456137	–	4088350	134	
15.8921	15.8985	628990	1	0.0064	4p 2 2	–	4d 1 4	3448887	–	4078130	14	
15.9535	15.9535	626822	6	0.0000	4p 3 1	–	4d 3 1	3396397	–	4023220	329	
15.9768	15.9757	625951	6	−0.0011	4p 2 1	–	4d 2 1	3389332	–	4015240	381	
16.0774	16.0774	621991	2b	0.0000	4p 1 1	–	4d 1 4	3456137	–	4078130	32	
16.1381	16.1370	619694	6	−0.0011	4p 2 2	–	4d 3 3	3448887	–	4068540	570	
16.1592	16.1592	618842	3	0.0000	4p 3 1	–	4d 2 1	3396397	–	4015240	81	
16.2419	16.2422	615680	2b	0.0003	4p 2 2	–	4d 1 3	3448887	–	4064580	22	
16.2566	16.2568	615127	8	0.0002	4p 3 1	–	4d 4 1	3396397	–	4011530	858	
	16.3214	612693	9									CdXX
16.3829	16.3884	610188	1	0.0055	4p 2 3	–	4d 2 3	3477956	–	4088350	24	
16.4354	16.4373	608372	3	0.0019	4p 1 1	–	4d 1 3	3456137	–	4064580	144	
16.5014	16.4981	606130	2	−0.0033	4p 1 2	–	4d 2 3	3482340	–	4088350	90	
16.6845	16.6821	599444	1	−0.0024	4f 3 4	–	4d 3 3	4667900	–	4068540	106	
16.7323	16.7324	597643	7	0.0001	4p 2 1	–	4d 1 1	3389332	–	3986980	229	
16.8819	16.8833	592301	2	0.0014	4f 4 2	–	4d 4 1	4603880	–	4011530	127	
16.9044	16.9045	591558	3	0.0001	4p 1 1		4d 0 1	3456137	–	4047700	89	
16.9324	16.9349	590497	3	0.0025	4p 2 3	–	4d 3 3	3477956	–	4068540	92	
17.0572	17.0568	586276	3	−0.0004	4p 2 2	–	4d 3 2	3448887	–	4035150	72	
17.1031	17.1057	584600	3	0.0026	4f 5 2	–	4d 5 1	4606060	–	4021720	173	
17.1255	17.1335	583652	3w	0.0080	4p 1 1	–	4d 2 2	3456137	–	4040060	56	
17.1750	17.1706	582391	2	−0.0044	4p 1 2	–	4d 1 3	3482340	–	4064580	37	
17.1892	17.1946	581578	4	0.0054	4f 3 1	–	4d 2 1	4597000	–	4015240	250	
17.2420	17.2420	579979	4w	0.0000	4f 4 1	–	4d 3 1	4603200	–	4023220	394	Tentative, Blend
17.2420				0.0000	4f 4 3	–	4d 3 3	4648520	–	4068540	797	Tentative, Blend
17.2548	17.2598	579381	2	0.0050	4f 3 4	–	4d 2 3	4667900	–	4088350	485	
17.3584	17.3583	576093	6	−0.0001	4f 5 1	–	4d 4 1	4587620	–	4011530	964	
	17.3817	575318	10									CdXX
17.4114	17.4122	574310	5	0.0008	4p 4 1	–	4d 4 2	3467062	–	4041400	234	
17.4283	17.4265	573839	3	−0.0018	4f 3 1	–	4d 3 1	4597000	–	4023220	225	
17.4347	17.4401	573391	2	0.0054	4f 3 2	–	4d 3 2	4608720	–	4035150	118	
17.5852	17.5798	568835	3	−0.0054	4f 3 3	–	4d 2 4	4660660	–	4092000	502	Blend
17.5852				−0.0054	4f 3 2	–	4d 2 2	4608720	–	4040060	384	Blend
17.5830				−0.0032	4f 4 2	–	4d 3 2	4603880	–	4035150	521	Blend
17.6097	17.6040	568053	4	−0.0057	4f 4 4	–	4d 3 4	4666370	–	4098500	683	
17.6163	17.6142	567724	4	−0.0021	4p 3 3	–	4d 3 4	3530843	–	4098500	151	
17.6377	17.6372	566983	5	−0.0005	4p 0 1	–	4d 1 4	3511162	–	4078130	135	
17.6828	17.6831	565512	4	0.0003	4f 5 3	–	4d 4 3	4651300	–	4085780	951	Blend
17.6878				−0.0047	4p 1 2	–	4d 0 1	3482340	–	4047700	10	Blend
17.7098	17.7098	564659	4	0.0000	4f 5 2	–	4d 4 2	4606060	–	4041400	794	
17.7276	17.7277	564089	6	0.0001	4f 6 1	–	4d 5 1	4585810	–	4021720	1118	
	17.7647	562914	7									CdXX
17.7885	17.7902	562107	3p	0.0017	4f 3 3	–	4d 3 4	4660660	–	4098500	89	Blend
17.7903				−0.0001	4p 2 3	–	4d 2 2	3477956		4040060	220	Blend
	17.8004	561785	6									CdXX
17.9050	17.8922	558903	4w	−0.0128	4p 1 3	–	4d 2 4	3533498	–	4092000	248	
17.9301	17.9342	557594	2s	0.0041	4p 1 2	–	4d 2 2	3482340	–	4040060	94	Blend
17.9370				−0.0028	4p 3 3	–	4d 2 3	3530843	–	4088350	18	Blend
17.9471	17.9470	557196	4	−0.0001	4p 2 3	–	4d 3 2	3477956	–	4035150	292	
17.9540	17.9559	556920	5	0.0019	4p 2 4	–	4d 3 4	3541520	–	4098500	434	
17.9805	17.9827	556090	3	0.0022	4p 4 1	–	4d 3 1	3467062	–	4023220	41	CdXIX
17.9986	17.9929	555775	3s	−0.0057	4f 3 1	–	4d 4 2	4597000	–	4041400	30	
18.0226	18.0197	554948	7	−0.0029	4p 3 2	–	4d 4 2	3486540	–	4041400	530	Blend
18.0201				−0.0004	4p 3 3	–	4d 4 3	3530843	–	4085780	735	Blend
18.0291	18.0286	554674	7	−0.0005	4p 4 1	–	4d 5 1	3467062	–	4021720	897	
18.0662	18.0668	553501	1	0.0006	4p 3 2	–	4d 2 2	3486540	–	4040060	18	
	18.0987	552525	10									CdXX
18.1660	18.1663	550470	3	0.0003	4p 2 4	–	4d 2 4	3541520	–	4092000	146	
18.2279	18.2275	548621	4p	−0.0004	4p 3 2	–	4d 3 2	3486540	–	4035150	185	
18.3666	18.3652	544508	1	−0.0014	4p 4 1	–	4d 4 1	3467062	–	4011530	61	

integrals R^k and ζ_{nl} bound with electrostatic and spin–orbit interactions are processed as adjustable parameters P determined by least-squares fit from $N_{\rm lev}$ known experimental energy levels ($N_{\rm lev} > N_{\rm par}$) of an electronic configuration in the studied ion. Initially separate studies of the spectra from ZnIII till BrVIII had led to accurate values of angular coefficients $\partial E/\partial P$ in intermediate coupling. This made possible a comprehensive survey of $3d^9$4s, -4p and -4d by means of generalized least squares (GLS) from levels of all ions simultaneously, aiming to increase the ratio $N_{\rm lev}/N_{\rm par}$. For that purpose, the electrostatic Slater parameters were replaced by $R^k = A(R^k) + B(R^k)\cdot Z_{\rm c} + C(R^k)/(Z_{\rm c} + D)$ according to Edlén [18] ($Z_{\rm c}$ = charge of the ionic core) and the spin–orbit parameters were expressed as polynomials $\zeta_{nl} = c_0 + c_1\cdot Z_{\rm c} + \cdots + c_4\cdot Z_{\rm c}{}^4$. The GLS constants $A(R^k)$, $B(R^k)$, $C(R^k)$ and c_i fitted from the sequence ZnIII–BrVIII were used to predict levels of ions till MoXV [19] and, after their discovery [20], till SnXXIII [21]. This guided the search for new levels beyond MoXV and the classification of 17 lines as 4s-4p transitions and 2 lines as 4p-4d transitions in laser produced plasma spectra of cadmium [9] were derived from these GLS studies. After 1988, the 4p-4d transitions of potential interest for soft X-ray lasers were surveyed [22], initial identifications of some $4d^1$S–$4p^1$P transitions were revised recently [2] and the KrIX spectrum was observed and interpreted at Troitsk [23].

Systematic discrepancies $\lambda_{\rm exp} - \lambda_{\rm GLS}$ had been noticed beyond MoXV in the wavelengths of 4p-4d transitions [21] and, in the present step, the reliability of the GLS levels was increased by using more stringent conditions and extended sets of experimental levels. The present study differs from earlier ones in two points:

1. The radial parameters were replaced by their scaling factors $SF(P) = P/P_{\rm HFR}$, by multiplying the angular coefficients $\partial E/\partial P$ by $P_{\rm HFR}$ values obtained from the RCN codes of Cowan [17]. It is a known fact that scaling factors are very consistent in neighboring elements and close to 1. First isoelectronic GLS studies in multicharged copper-like ions used successfully SF's as adjustable parameters [24].
2. The experimental error on the energies in the fit ranges from $0.3\,{\rm cm}^{-1}$ in ZnIII to $\sim 200\,{\rm cm}^{-1}$ for $Z_{\rm c} > 25$. Therefore the levels were weighted as ${Z_{\rm c}}^{-1}$.

The main features of the four GLS studies are collected in Table I. For $3d^9$4f, which uses some recent data on 4d-4f transitions [25], no GLS study had been performed.

The average of deviations $\Delta E = E_{\rm exp} - E_{\rm GLS}$ in column 5 increases from $3d^9$4s to $3d^9$4f, partly due to mixing with other configurations which are not considered in our "single" configuration model. $3d^9$4s and $3d^9$4p are isolated in all ions studied here, whereas $3d^9$4d is overlapped by $3d^9$5s and $3d^8$4s^2 at $Z_{\rm c} = 3, 4$ and $3d^9$4f by $3d^8$4s4p and $3d^9$np in several low-$Z_{\rm c}$ ions (see BrVIII [26]). In the latter configurations, the most perturbed levels were discarded in the fitting process. Two levels of $3d^9$4f with $J = 4$ are derived from a line at 17.242 nm. In the present step of GLS calculations, it was not possible to reduce the large deviations $E_{\rm exp} - E_{\rm GLS}$ with a reasonable set of fitted parameters and the classified line and levels are reported as tentative.

The predicted levels of CdXXI are collected in Table II and are compared with energies derived from the classified lines of Table III. For $3d^9$4s and $3d^9$4p, the energies are those of [9]. Two couplings are given and the $J_1 - j_2$ coupling leads generally to more realistic designations than does Russell–Saunders. In the recent publication [8] using the RMBPT method, the transition energies of Ni-like ions from Ag to Sn were reported for 3–4 resonance transitions, and for 4s-4p and 4p-4d transitions, except both $3d^9$4d $J = 0$ levels. For CdXXI, the published 4-4 transitions are close to $\lambda_{\rm exp}$ and $\lambda_{\rm GLS}$ values. For the 53 lines reported in Table III, the average deviation $\langle\lambda_{\rm exp} - \lambda_{\rm th}\rangle$ is 0.0080 nm for the relativistic MBPT method and 0.0065 nm for the present GLS study. In terms of energies $E_{\rm MBPT}$ relative to the ground state, systematic deviations appear.

Several cadmium lines are still uninterpreted and they might belong to other ions. Comparisons with the zinc-like lines reported in [9] were not conclusive. It is noticed that the strongest of those lines are close to 4-4 transitions of CdXXII as we derive them from scaled Cowan-type calculations. As the CoI isoelectronic sequence is too poorly known, this did not lead so far to definite conclusions.

4. Conclusions

Fifty-three transitions corresponding to Ni-like Cd ions have been identified from the spectra of high current capillary discharge plasma columns. The average deviation between the measured and theoretical wavelength values is $\langle\lambda_{\rm exp} - \lambda_{\rm th}\rangle = 0.0065$ nm for the GLS method used in the present study, as compared to 0.0080 nm for the MBPT method. The results demonstrate that fast capillary discharges can produce clean spectra for the study of multiply charged ions with charges of up to at least $Z = 20$. The newly identified Ni-like Cd lines can be used in combination with other Cd ion transitions reported in the literature in the plasma diagnostics necessary for the development of efficient Ni-like Cd lasers operating at a wavelength of 13.2 nm.

Acknowledgement

This work was supported by DARPA grant G_DAAD 19-99-1-0279 and by the National Science Foundation. The Colorado State University researchers also gratefully acknowledge the support from the W. M. Keck Foundation. The Laboratoire Aime Cotton is associated with Universite Paris-Sud. We acknowledge the contributions of Maximo Frati and Fernando Tomasel to the generation of the Cd capillary plasmas and thank V. N. Shlyaptsev for useful discussions.

References

1. Zhang, J. *et al.*, Phys. Rev. Lett. **78**, 3856 (1997).
2. Li, Y. *et al.*, Phys. Rev. A **58**, R2668 (1998).
3. Daido, H., Ninomiya, S., Takagi, M., Kato, Y. and Koike, F., J. Opt. Soc. Am B **16**, 296 (1999).
4. Dunn, J. *et al.*, Phys. Rev. Lett. **84**, 4834 (2000).
5. Spector, N. *et. al.*, J. Phys. B: At. Mol. Opt. Phys. **17**, L275 (1984).
6. Quinet, P. and Biémont, É., Physica Scripta **43**, 150 (1991).
7. Renaudin, P. *et al.*, in "UV and X-Ray Spectroscopy of Laboratory and Astrophysical Plasmas," (Eds. E. Silver and S. Kahn) (Cambridge University Press, 1993) p. 157.
8. Safronova, U. I., Johnson, W. R. and Albritton, J. R., Phys Rev. A **62**, 052505 (2000).

9. Churilov, S. S., Ryabtsev, A. N. and Wyart, J.-F., Physica Scripta **38**, 326 (1988).
10. Gonzalez, J. J., Frati, M., Rocca, J. J., Shlyaptsev, V. N. and Osterheld, A. L., Phys. Rev. E **65**, 026404 (2002).
11. Sakadzik, S. *et al*., Soc. Photo-Opt. Instrum. Eng. J. **4505**, 35 (2001).
12. Kelly, R. L., J. Phys. Chem. Ref. Data. **16**, 1 (1985), R. L. Kelly and L. J. Palumbo, "Atomic and Ionic Emission Lines Below 2000 Angstroms," NRL Report 7599 (1973).
13. Reader, J., Acquista, N. and Cooper, D., J. Opt. Soc. Am. B **73**, 1765 (1983).
14. Ivanov, L. N., Ivanova, E. P., Kononov, E. Ya., Churilov, S. S. and Tsirekidze, M. A., Physica Scripta **33**, 401 (1986).
15. Seely, J. F., Brown, C. M. and Feldman, U., At. Data Nucl. Data Tab. **43**, 145 (1989).
16. Bordarier, Y., Bachelier, A. and Sinzelle, J., Chain of Programs AGENAC, ASSAC, DIAGAC, GRAMAC, Laboratoire Aimé Cotton, Orsay (1980).
17. Cowan, R. D., "The Theory of Atomic Structure and Spectra," (University of California Press, Berkeley, 1981) and computer codes.
18. Edlén, B., in "Encyclopedia of Physics," Vol. XXVII, Springer Verlag, Berlin (1964).
19. Wyart, J.-F. and Ryabtsev, A. N., Physica Scripta **33**, 215 (1986).
20. Ryabtsev, A. N., Churilov, S. S. and Wyart, J.-F., Opt. I. Spektr. **62**, 258 (1987).
21. Wyart, J.-F., Physica Scripta **36**, 234 (1987).
22. Scofield, J. H. and MacGowan, B. J., Physica Scripta **46**, 361 (1992).
23. Ryabtsev, A. N., Antsiferov, P. S., Nazarenko, V. I., Churilov, S. S. and Wyart, J.-F., J. Physique IV, **11**, 317, (2000).
24. Wyart, J.-F., Ryabtsev, A. N. and Reader, J., J. Opt. Soc. Am. **71**, 692 (1981).
25. Ryabtsev, A. N. *et al*., Opt. I. Spektr. **87**, 197 (1999).
26. Churilov, S. S. and Joshi, Y. N., Physica Scripta **53**, 431 (1996).

Classification of the Nickel-like Silver Spectrum from a Fast Capillary Discharge Plasma

A. Rahman [1], J.J. Rocca [1,2] and J.-F. Wyart[3]

[1]Department of Electrical and Computer Engineering
[2]Department of Physics,
Colorado State University. Fort Collins, CO 80523
[3]Laboratoire Aimé Cotton, CNRS (UPR 3321),
Centre Universitaire, 91405-Orsay, France

: 32.30,32.70,42.55.

Abstract

The study of the Ni-like silver (AgXX) spectra in the 13.7 -20.5 nm wavelength region using a plasma generated by a fast high power capillary discharge is reported. Forty-three AgXX transitions have been identified with the assistance of calculations performed using the Slater-Condon method with generalized least-squares fits of the energy parameters. The average difference between the measured transition wavelengths and the theoretical values is 0.0026 nm.

1. Introduction

Capillary discharge excitation has proven to be an efficient method to create very compact lasers in the 46.9-60.8 nm spectral region using Neon-like ions [1-3]. Several applications demand lasers at even shorter wavelengths. In particular, the metrology associated with extreme ultraviolet lithography for the fabrication of the future generations of integrated circuits motivates the development of lasers emitting at wavelengths in the vicinity 13.5 nm [4]. Lasing at 13.9 and 13.2 nm in the $3d^9\ 4d\ ^1S_0$ - $3d^9\ 4p\ ^1P_1$ transitions of nickel-like silver [5-10] and cadmium [8] respectively has been observed in laser-created plasmas. Also lasing was observed on the 4f $^1P_1$ - 4d $^1P_1$ transition of AgXX at 16.05 nm [10]. The further development of practical lasers operating in this wavelength region generates significant interest in the spectra of these Ni-like ions. Recently, a detailed spectroscopic study of Ni-like Cd has been reported utilizing a capillary discharge plasma [11]. Numerous newly identified Ni-like cadmium transitions were observed and classified in the 12.7-18.4 nm wavelength region in a cadmium plasma excited by such a discharge.

Rocca@engr.colostate.edu

Francois.Wyart@lac.u-psud.fr

Herein we report the use of a similar discharge in silver vapor to study the spectra of Ni-like silver in the spectral region between 12.7 and 20.5 nm. The highly ionized Ag plasma was obtained with fast capillary discharge excitation of a silver vapor filled capillary channel with discharge current pulses up to 200 kA peak amplitude and rise time of approximately 1.5×10^{13} A/sec. Previous work in laser-created plasmas [12] has identified five AgXX lines in the 17.0-19.0 nm spectral region as 4p-4d transitions, in addition to 18 lines of the $3d^9 4s$-$3d^9 4p$ array from 24.8 to 31.8 nm. In the present spectra, all previously reported 4d-4p and 4d-4f transitions of AgXIX [13] and AgXX were strong emission lines and this was an incentive to extend the classification to weaker lines.

The plasma generation technique and the set-up utilized in the acquisition of the spectra are discussed in the next section. Section 3 discusses the theoretical computation and the line assignments.

2. Experimental set-up

The highly ionized silver plasmas of interest were generated by rapid electromagnetic compression of a silver vapor plasma column in a capillary channel. In these types of plasmas the contrast between the line and continuum spectra can be significantly larger than in laser created plasma, facilitating the classification of bound-bound atomic transitions. The silver vapor was created by heating and vaporizing a silver electrode with a current pulse. The metal vapor produced by this room-temperature metal vapor gun was injected through a hollow electrode into a 5 mm diameter, 4 cm long channel drilled into a polyacethal rod. The silver vapor injected into the channel was pre-ionized using a moderate current pulse and was subsequently compressed and heated using a fast high current pulse of 160- 200 kA peak amplitude and ~ 12-15 ns risetime. The high current pulse was produced using a three stage pulse-compression system consisting of a conventional eight-stage Marx generator, followed by a 26 nF cylindrical water dielectric capacitor and a radial water-dielectric Blumlein transmission line [14]. The Marx generator was operated at an erected voltage of ~ 650 kV to charge the water dielectric capacitor that in turn was discharged through a self-breaking spark-gap pressurized with SF_6 gas to pulse charge the transmission line. The Blumlein transmission line was discharged through the capillary channel located on its axis triggering an array of seven synchronously triggered spark-gaps. Each stage of pulse compression enables the generation of

current pulses of increasingly shorter risetimes, allowing the creation of very fast current risetimes with a current increase rate that exceeds 1.5×10^{13} A/s. The Lorentz force associated with the current pulse rapidly compresses and heats the plasma, generating a narrow plasma column on axis, which reaches the Ni-like stage of ionization. Maximum soft x-ray emission occurs when the column pinches on axis. Pinhole camera measurements of cadmium plasma columns excited under similar discharge conditions show that at this time the soft x-ray emitting region has a diameter of 250-350 um. Shortly after, the soft x-ray emission decreases as the plasma column expands and rapidly cools [15].

Plasma radiation emitted through axial holes in the ground electrode and metal vapor gun was collected and focused onto the slit of a 2.217 m grazing incidence spectrograph using a gold-coated cylindrical mirror placed at a grazing angle of 85.8 degrees. The radiation was dispersed by a 2400 lines/mm gold-coated grating mounted at an angle of incidence of 85.8 degrees along the perimeter of a Rowland circle. The first order diffracted beam was recorded by a two-dimensional array detector system. This detector consists of two micro-channel plates (MCP's) mounted in a chevron configuration, a fiber optics plate coated with phosphorous, and a 1024X1024 pixels CCD camera. The MCP's were gated with a resolution of ~ 5 ns to allow the recording of spectra corresponding to different times of the plasma column evolution. Figure 1 shows typical spectra of capillary discharge silver plasma for the 16.2-19.4 nm wavelength region. Calibration of the spectral region between 12.80-14.00 nm was performed using known transitions of OVI, OVII, ArVIII and FVI[16]. A second spectral region of interest, covering the wavelength range between 16.5 and 20.5 nm was calibrated using various known Argon transitions (ArIX through ArXIV) and OVI lines [16]. The calibration was verified by acquiring highly ionized silver spectra and comparing them with previously known lines of AgXIX and AgXX. The measured values of AgXIX lines averaged over several shots were found to deviate by less than 0.004 nm from those previously reported in the literature [13]. The maximum deviation between the AgXX lines reported in the literature [12] and the values measured in the present experiment was found to be 0.013 nm. From these comparisons, from the difference between the wavelength of other known lines and those obtained applying the calibration curve, and from shot to shot variations of the measured wavelengths, the error in the measurement of the transition wavelengths reported herein can be conservatively estimated at 0.01 nm.

3. Interpretation of the silver spectra

The same theoretical methods previously used to classify lines from CdXXI [11] was used for AgXX. The advantages of the Generalized least-squares (GLS) techniques for improving the reliability of multicharged ions predicted energies in the framework of the Racah-Slater method had been stressed in ref [11] and will not be repeated. Isoelectronic constraints were applied to the scaling factors of radial parameters of the four excited configurations $3d^9 4l$ (l=s,p,d,f). The scaling factor is the ratio of an 'adjustable' radial parameter to its *ab initio* (HFR) value, which is derived from the RCN, RCN2 codes by R.D. Cowan [17]. The experimental 4s and 4p levels used in the GLS fits were those of [12] and earlier references. For $3d^9 4d$, the set of E_{exp} values was extended from 228 values in [12] to 239 after inclusion of the new AgXX levels in the final fit. The predicted levels of AgXX are collected in Table I and are compared with energies derived from the classified lines of Table II. As for the case of CdXXI, the (J_1,j_2) coupling is a better approximation than is LS and the changes in leading components are small in those close elements.

4. Conclusions.

A highly ionized silver plasma generated by a fast high current capillary discharge was used to identify fortry-three transitions of Ni-like Ag. The average deviation between the measured and theoretical transition wavelength values is 0.0026 nm. The newly identified lines can be of use in the plasma diagnostic necessary to optimize the performance of Ni-like Ag lasers operating at 13.9 nm.

Acknowledgments

This work was supported by DARPA grant G-DAAD 19-99-1-0279 and by the National Science Foundation. The Laboratoire Aimé Cotton is associated with the University Paris-Sud. We also would like to thank Eric Hammarsten for his assistance with the experiment and acknowledge an equipment grant from the W.M. Keck foundation to Colorado State University.

Figure Caption:

Figure1.(a-c) Spectra of capillary discharge silver plasma for the 16.2-19.4 nm wavelength region. Each spectrum corresponds to a single discharge shot and was acquired with a time resolution of about 5 ns. The capillary diameter was 5 mm and the discharge current pulse had a peak amplitude of 167 kA, 167 kA and 164 kA respectively. Each spectral line is identified with the experimental wavelength corresponding to that particular discharge shot. The difference in wavelength of the lines appearing in the overlapping regions are illustrative of the error associated with the measurements. Notice that the experimental wavelengths listed in Table II are the result of averaging several spectra. Some of the weak lines listed in Table II which do not appear clearly in these spectra were classified based on their identification in the spectra corresponding to other discharge shots.

Table I

Energy levels of AgXX. Levels are designated in the (J_1,j_2) coupling scheme with J and N index numbering from the lowest level in its J-value for the configuration. The (J_1,j_2) purity in % is followed by SL leading components and purities. Energy values are in cm^{-1}

Config.	Multiplet	J	N^{th}	%	SL	%	E_{exp}	E_{GLS}
$3d^{10}$		0	1		^1S	100	0	0
$3d^9 4s$	(5/2,1/2)	3	1	100	^3D	100	2807885	2807855
	(5/2,1/2)	2	1	99	^3D	51	2814345	2814304
	(3/2,1/2)	1	1	100	^3D	100	2859060	2859074
	(3/2,1/2)	2	2	99	^1D	51	2864395	2864451
$3d^9 4p$	(5/2,1/2)	2	1	96	^3P	67	3122417	3122540
	(5/2,1/2)	3	1	99	^3F	50	3129393	3129309
	(3/2,1/2)	2	2	93	^3F	85	3175562	3175607
	(3/2,1/2)	1	1	71	^3P	58	3181814	3181734
	(5/2,3/2)	4	1	100	^3F	100	3191211	3191162
	(5/2,3/2)	2	2	90	^1D	62	3201870	3201870
	(5/2,3/2)	1	2	69	^1P	82	3206188	3206250
	(5/2,3/2)	3	2	99	^3D	74	3209891	3209772
	(3/2,3/2)	0	1	100	^3P	100	3229410	3229433
	(3/2,3/2)	3	3	100	^3F	49	3248295	3248421
	(3/2,3/2)	1	3	92	^3D	59	3251230	3251044
	(3/2,3/2)	2	4	98	^3D	57	3258589	3258728
$3d^9 4d$	(5/2,3/2)	1	1	69	^3S	79	3687150	3687297
	(5/2,3/2)	4	1	98	^3D	57	3710770	3710662
	(5/2,3/2)	2	1	87	^3P	51	3714000	3714179
	(5/2,3/2)	3	1	89	^3D	44	3721590	3721435
	(5/2,5/2)	1	2	71	^1P	51	3719060	3718862
	(5/2,5/2)	5	1	100	^3G	100	3719430	3719454
	(5/2,5/2)	3	2	88	^3D	39	3732080	3732215
	(5/2,5/2)	2	2	83	^1D	39	3737110	3736977
	(5/2,5/2)	4	2	98	^3F	78	3738070	3738186
	(5/2,5/2)	0	1	50	^3P	99	3743390	3743026
	(3/2,3/2)	1	3	69	^1P	47	3757490	3757758
	(3/2,3/2)	3	3	93	^3G	74	3761440	3761250
	(3/2,3/2)	2	3	96	^3F	71	3780240	3780364
	(3/2,3/2)	0	2	51	^1S	99	3926590	3926657

	(3/2,5/2)	1	4	68	^{3}D	56	3769630	3769578
	(3/2,5/2)	4	3	98	^{1}G	41	3777140	3777078
	(3/2,5/2)	2	4	93	^{3}D	41	3783160	3783151
	(3/2,5/2)	3	4	97	^{3}F	53	3788660	3788801
$3d^9 4f$	(5/2,5/2)	0	1	100	^{3}P	100		4237753
	(5/2,5/2)	1	1	78	^{3}P	90	4242500	4242766
	(5/2,5/2)	2	1	69	^{3}P	64		4250992
	(5/2,5/2)	5	1	97	^{3}H	55	4257030	4257022
	(5/2,5/2)	3	1	57	^{3}D	54	4265930	4266009
	(5/2,5/2)	4	1	70	^{3}F	77	4270140	4269009
	(5/2,7/2)	6	1	100	^{3}H	100	4255340	4254974
	(5/2,7/2)	2	2	74	^{1}D	40		4264980
	(5/2,7/2)	4	2	67	^{1}G	47	4271600	4272036
	(5/2,7/2)	5	2	96	^{3}G	76	4274400	4274068
	(5/2,7/2)	3	2	56	^{1}F	48	4276548	4276293
	(5/2,7/2)	1	2	48	^{3}D	85	4283940	4283578
	(3/2,7/2)	2	3	85	^{3}D	37		4304534
	(3/2,7/2)	4	3	93	^{3}H	73	4310257	4310013
	(3/2,7/2)	5	3	97	^{3}H	39	4313940	4313746
	(3/2,7/2)	3	4	98	^{3}G	63	4329060	4328895
	(3/2,5/2)	2	4	90	^{3}F	63		4317844
	(3/2,5/2)	3	3	99	^{3}F	41	4322160	4322284
	(3/2,5/2)	4	4	95	^{3}G	45	4326960	4327415
	(3/2,5/2)	1	3	66	^{1}P	93	4381930	4382027

Table II.

Classification of lines of Nickel-like AgXX. The first column shows the calculated wavelengths (λ_{cal} in nm) as they are derived from the "best" experimental values in Table I. The second and third column show the experimental wavelengths (λ_{exp}) and wavenumber. Int is the measured relative intensity. The level designations imply the J-value and index N_{th} which numbers the levels from the lowest energy in the same J-value and configuration as used in [12]. The emission transition probability gA (in 10^9 s^{-1}) in length form is derived by means of Cowan codes for E_{GLS} level values with no C.I. effects included.

λ_{cal}(nm)	λ_{exp}(nm)	λ (cm^{-1})	Int	λ_{exp}-λ_{cal}	J_0 N_{th}	J_e N_{th}	E_{odd}	E_{even}	gA	Comment
13.4269	13.4250	744879	1	-0.0019	4p 1 1	4d 2 0	3181814	3926590	16	
13.8811	13.8830	720305	7	0.0011	4p 1 2	4d 0 2	3206188	3926590	153	
16.5377	16.5390	604617	2	0.0013	4p 2 2	4d 2 3	3175562	3780240	198	
16.5924	16.5919	602704	2	-0.0005	4p 3 1	4d 3 2	3129393	3732080	46	Tentative,AgXXI
16.6898	16.6898	599168	3	0.000	4p 2 1	4d 3 1	3122417	3721590	249	
16.7105	16.7122	598365	3	0.0017	4p 1 1	4d 2 3	3181814	3780240	100	Tentative,AgXXI
16.8863	16.8870	592171	4	-0.0007	4p 3 1	4d 3 1	3129393	3721590	286	
16.9038	16.8995	591733	4	-0.0043	4p 2 1	4d 2 1	3122417	3714000	347	
17.0684	17.0704	585809	5	0.0020	4p 2 2	4d 3 3	3175562	3761440	517	
17.1055	17.1088	584495	2	0.0033	4p 3 1	4d 2 1	3129393	3714000	73	Tentative,AgXXI
17.2005	17.2039	581264	6	-0.0034	4p 3 1	4d 4 1	3129393	3710770	797	
17.3709	17.3752	575533	1	0.0043	4p 1 1	4d 1 3	3181814	3757490	125	
17.4200	17.4152	574211	3	-0.0048	4p 1 2	4d 2 3	3206188	3780240	94	
17.6174	17.6213	567495	3	0.0039	4d 3 3	4f 3 4	3761440	4329060	97	S
17.7075	17.7074	564736	4	-0.0001	4p 2 1	4d 1 1	3122417	3687150	210	
17.7029	17.7074	564736	4	0.0045	4d 1 2	4f 1 2	3719060	4283940	99	Tentative,AgXXI
17.8070	17.8070	561577	1	0.000	4p 1 1	4d 0 1	3181814	3743390	85	Tentative, Blend
17.8079	17.8070	561577	1	-0.0009	4p 2 2	4d 2 2	3175562	3737110	28	Tentative, Blend
17.8336	17.8377	560610	2	0.0041	4d 4 1	4f 4 2	3710860	4271600	140	
17.8709	17.8688	559635	2	-0.0021	4p 2 3	4d 3 3	3201870	3761440	95	
17.9689	17.9670	556576	1	-0.0019	4p 2 2	4d 3 2	3175562	3732080	78	
18.0190	18.0216	554890	1b	0.0026	4d 5 1	4f 5 2	3719430	4274400	161	
18.1182	18.1182	551931	2b	0.000	4d 2 1	4f 3 1	3714000	4265930	248	
18.1815	18.1773	550137	3	-0.0042	4d 3 1	4f 4 2	3721590	4271600	194	
18.2209	18.2205	548832	4b	-0.0004	4d 3 3	4f 4 3	3761440	4310260	747	Tentative, Blend
18.2209	18.2205	548832	4b	-0.0004	4d 2 3	4f 3 4	3780240	4329060	442	Tentative, Blend
18.2299	18.2205	548832	4b	-0.0094	4d 3 1	4f 4 1	3721590	4270140	315	Tentative, Blend
18.2862	18.2868	546849	2	0.0006	4p 4 1	4d 4 2	3191211	3738070	219	
18.3092	18.3094	546174	5	0.0002	4d 4 1	4f 5 1	3710860	4257030	902	
18.3665	18.3803	544040	1b	0.0138	4d 3 2	4f 3 2	3732080	4276550	122	Tentative, Blend
18.3709	18.3803	544040	1b	0.0094	4d 3 1	4f 3 1	3721590	4265930	227	Tentative, Blend

18.3942	18.3941	543653	5	-0.0001	4d 3/2	4f 5/2	892277	1435920	521	AgXIX
18.5048	18.5088	540284	2b	0.0040	4d 3 4	4f 3 4	3788660	4329060	60	Tentative, Blend
18.5060	18.5088	540284	2b	0.0028	4p 3 3	4d 3 4	3248295	3788660	142	Tentative, Blend
18.5110	18.5152	540097	2b	0.0042	4p 0 1	4d 1 4	3229410	3769630	126	
18.5350	18.5309	539639	1b	0.0041	4d 3 2	4f 4 2	3732080	4271600	436	q
18.5378	18.5378	539438	1b	0.000	4d 2 2	4f 3 2	3737110	4276550	373	q
18.5530	18.5530	538996	2	0.000	4d 2 4	4f 3 3	3783160	4322160	450	
18.5770	18.5770	538300	2	0.000	4d 3 4	4f 4 4	3788660	4326960	640	
18.6134	18.6166	537155	1b	0.0032	4p 1 2	4d 1 2	3181814	3719060	43	
18.6290	18.6290	536797	3b	0.000	4d 4 3	4f 5 3	3777140	4313940	894	
18.6451	18.6451	536334	4	0.000	4d 4 2	4f 5 2	3738070	4274400	747	
18.6599	18.6599	535909	4	0.000	4d 5 1	4f 6 1	3719430	4255340	1060	
18.7319	18.7341	533786	1b	0.0022	4d 3 2	4f 3 1	3732080	4265930	64	q
18.7441	18.7415	533575	2b	-0.0026	4d 3 4	4f 3 3	3788660	4322160	83	
18.7753	18.7719	532711	7	-0.0034	4d 5/2	4f 7/2	904224	1436839	705	AgXIX
18.7995	18.8046	531786	2	-0.0051	4p 1 3	4d 2 4	3251230	3783160	205	AgXIX
18.8352	18.8368	530876	2	0.0016	4p 1 2	4d 2 2	3206188	3737110	82	
18.8605	18.8626	530150	4	0.0021	4p 2 3	4d 3 2	3201870	3732080	271	Tentative, Blend
18.8654	18.8626	530150	4	-0.0028	4p 2 4	4d 3 4	3258589	3788660	405	Tentative, Blend
18.9092	18.9092a	528843	7c	0.000	4p 3 3	4d 4 3	3248295	3777140	693	
18.9315	18.9315a	528220	7c	0.000	4p 4 1	4d 5 1	3191211	3719430	851	
18.9330	18.9230a	528457	7c	-0.0100	4p 3 2	4d 4 2	3209891	3738070	496	
18.9674	18.9704	527137	4	0.0030	4p 3 2	4d 2 2	3209891	3737110	15	S
19.0632	19.0519	524882	8	-0.0112	4p 2 4	4d 2 4	3258589	3783160	147	AgXIX
19.1502	19.1501	522190	2	0.000	4p 3 2	4d 3 2	3209891	3732080	159	
19.4980	19.4956	512936	5	-0.0024	4p 1 2	4d 1 2	3206188	3719060	103	AgXIX
19.5427	19.5420	511718	1	-0.0007	4p 3 2	4d 3 1	3209891	3721590	98	

Notes: a Wavelength from ref [11]. The present spectra lead to an unresolved peak with global intensity 7

S line is too strong with regard to the gA value

XXI probably coincident with a transition of higher charged ion.

XIX blend with a classified line of Cu-like Ag XIX

q this line did not appear in all spectra

b broad line

c only combined intensity can be assigned for all three transitions

References

1. J.J. Rocca**,** V. N. Shlyaptsev, F.G.Tomasel, O.D.Cortazar, D. Hartshorn, J.L.A. Chilla, Phys. Rev. Lett., **73**, 2192 (1994).
2. F.G. Tomasel, J.J. Rocca, V.N. Shlyaptsev and C.D. Macchietto, Phys. Rev. A, **55**, 1437 (1997).
3. M. Frati, M. Seminario and J.J. Rocca , Optics. Lett. **25**, 1022, (2000).
4. D.T. Attwood. "Soft x-rays and extreme ultraviolet radiation". Cambridge University Press. (1999).
5. Y. Li, J. Nilsen, J. Dunn, A.L. Osterheld, A.N. Ryabtsev and S.S. Churilov, Phys. Rev. A, **58**, 2668 (1998).
6. J. Zhang et al. Phys. Rev. Letters, **78**, 3856 (1997)
7. P. Warwick et al., IEEE J. of Selected Topics in Quantum Electronics, **5** , 1447, (1999).
8. J. Dunn et al., Phys. Rev. Letters, **84**, 4834 (2000).
9. A. Klisnick et al., J. Opt. Soc. Am. B, **17**, 1093 (2000)
10. J. Kuba et al., Phys. Rev. A 62, 043808 (2000).
11. A. Rahman, E.C. Hammarsten, S. Sakadzic, J.J. Rocca, and J.-F. Wyart, Phys. Scripta, **67**, 414 (2003).
12. S.S. Churilov, A.N. Ryabstev, and J.-F. Wyart, Phys. Scripta, **38**, 326, (1988).
13. J. Reader, N. Acquista and D.N. Cooper, J. Opt. Soc. Am. **73**, 1765 (1983).
14. J.J. Gonzalez, M. Frati, J.J. Rocca, V.N. Shlyaptsev and A. Osterheld. Phys. Rev. E. **65,** 026404 (2002)
15. A. Rahman, E.C. Hammarsten, S. Sakadzic, V.N. Shlyaptsev, A. Osterheld and J.-F. Wyart. P 113 "X-Ray Lasers 2002", AIP conf. Proceed. 641 Eds. J.J. Rocca, J. Dunn and S. Suckewer (2002).
16. R.L. Kelly, L.J. Palumbo, *Atomic and Ionic Emission Lines Below 2000 Angstroms*, NRL Report 7599 (1973).
17. R.D. Cowan, *The Theory of Atomic Structure and Spectra*, University of Calif. Press, Berkeley (1981) and computer codes.

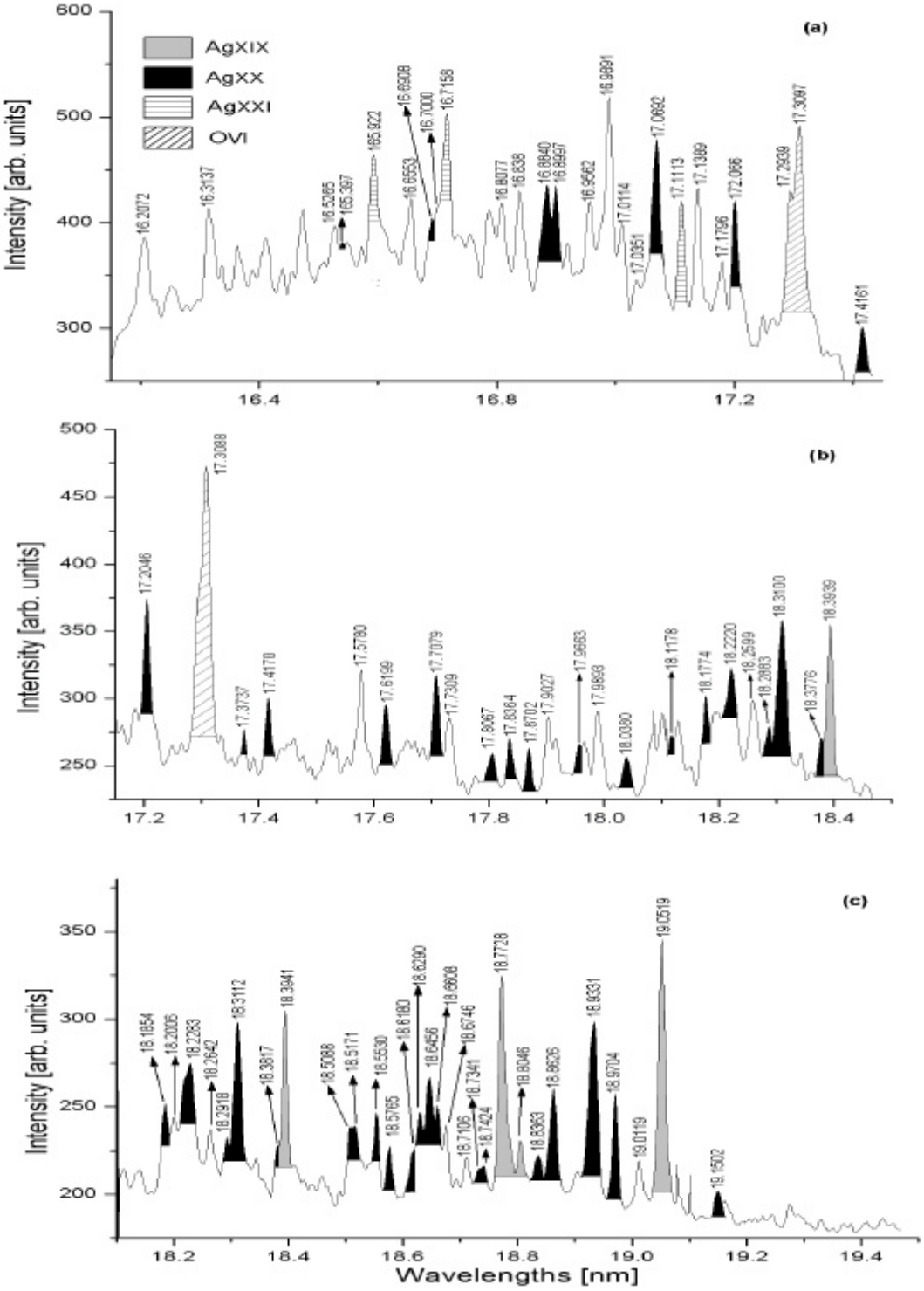
(a)
AgXIX
AgXX
AgXXI
OVI
Intensity [arb. units]
(b)
Intensity [arb. units]
(c)
Intensity [arb. units]
Wavelengths [nm]

Figure 1